Summer 8-14-2020

Triclosan Disrupts Immune Cell Function by Depressing Ca2+ Influx via Acidification of the Cytoplasm

Suraj Sangroula
University of Maine, suraj.sangroula@maine.edu

TRICLOSAN DISRUPTS IMMUNE CELL FUNCTION BY DEPRESSING CA^{2+} INFLUX VIA ACIDIFICATION OF THE CYTOPLASM

By

Suraj Sangroula

B.S. University of New Hampshire, 2017

A DISSERTATION

Submitted in Partial Fulfillment of the

Requirements for the Degree of

Master of Science

(in Biochemistry)

The Graduate School

The University of Maine

August 2020

Advisory Committee:

Julie A. Gosse, Associate Professor of Biochemistry, Advisor

Robert Gundersen, Associate Professor of Biochemistry

Samuel T. Hess, Associate Professor of Physics

TRICLOSAN DISRUPTS IMMUNE CELL FUNCTION BY DEPRESSING CA^{2+} INFLUX VIA ACIDIFICATION OF THE CYTOPLASM

By Suraj Sangroula

Dissertation Advisor: Dr. Julie A. Gosse

An Abstract of the Dissertation Presented
in Partial Fulfillment of the Requirements for the
Degree of Master of Science
(in Biochemistry)
August 2020

Triclosan (TCS) is an antimicrobial agent that was effectively banned by the FDA from hand soaps in 2016, hospital soaps in 2017, and hand sanitizers in 2019; however, TCS can still be found in a few products. At consumer-relevant, non-cytotoxic doses, TCS inhibits the functions of mitochondria and mast cells, a ubiquitous cell type. Via the store-operated Ca^{2+} entry mechanism utilized by many immune cells, mast cells undergo antigen-stimulated Ca^{2+} influx into the cytosol, for proper function. Previous work showed that TCS inhibits Ca^{2+} dynamics in mast cells, and here we show that TCS also inhibits Ca^{2+} mobilization in human Jurkat T cells. However, the biochemical mechanism behind the Ca^{2+} dampening has yet to be elucidated. Three-dimensional super-resolution microscopy reveals that TCS induces mitochondrial swelling, in line with and extending the previous finding of TCS inhibition of mitochondrial membrane potential via its proton ionophoric activity. Inhibition of plasma membrane potential (PMP) by the canonical depolarizer gramicidin can inhibit mast cell function. However, use of the genetically encoded voltage indicators (GEVIs) ArcLight (pH-sensitive) and ASAP2 (pH-

insensitive), indicates that TCS does not disrupt PMP. In conjunction with data from a plasma membrane-localized, pH-sensitive reporter, these results indicate that TCS, instead, induces cytosolic acidification in mast cells and T cells. Acidification of the cytosol likely inhibits Ca^{2+} influx by uncoupling the STIM1/ORAI1 interaction that is required for opening of plasma membrane Ca^{2+} channels. These results provide a mechanistic explanation of TCS disruption of Ca^{2+} influx and, thus, of immune cell function.

ACKNOWLEDGEMENTS

First, I would like to thank Dr. Julie Gosse for mentoring me for the past 3 years. I am forever grateful to her for believing in me and providing me with the opportunity to do this research project. She has helped me improve various professional and scientific skills such as developing experiments, troubleshooting problems and scientific writing. Dr. Gosse provided me with continuous encouragement through the ups and downs of this project. None of my work would have been possible without her.

I would like to thank my committee members Drs. Julie Gosse, Robert Gundersen and Samuel T. Hess for their valuable feedbacks and guidance in this project.

I would like to specially thank Prakash Raut, Dr. Matthew Parent, Dr. Samuel Hess and all other members of Hess lab for their technical help and discussion for the FPALM part of this project. I would also like to thank Dr. Robert Wheeler, Siham Hattab, and Bailey Blair for use of and help with the ibidi heating system and confocal microscope; Dr. Joshua Kelley, William Simke, and Andrew Hart for help with image analysis and widefield microscope; Dr. Lili Wang for helpful discussions regarding imaging Jurkat T cells; and Dr. Jaime de Juan Sanz and Dr. Francois St-Pierre for helpful discussions regarding genetically encoded voltage indicators.

I would like to thank Dr. Juyoung Shim for training me with laboratory techniques that helped me do my experiments. I would like to thank Alan Y. Baez Vasquez, who contributed significantly in this project. I would also like to thank Bright Obeng, Grace D. Bagley, Bailey E. West, Christian M. Potts, Marissa S. Kinney, Sasha R. Weller and John E. Burnell for their contributions in this project and help in running the lab smoothly.

The manuscript for this project has been submitted for publication in the *Toxicology and Applied Pharmacology* journal. The full title and author list for the manuscript is "Triclosan Disrupts Immune Cell Function by Depressing Ca^{2+} Influx Following Acidification of the Cytoplasm," by Suraj Sangroula, Alan Y. Baez Vasquez, Prakash Raut, Bright Obeng, Juyoung K. Shim, Grace D. Bagley, Bailey E. West, John. E. Burnell, Marissa S. Kinney, Christian M. Potts, Sasha R. Weller, Joshua B. Kelley, Samuel T. Hess, Julie A. Gosse.

Lastly, I would like to thank all of my family, friends, mentors and teachers who have supported and encouraged me throughout my academic career.

This research was supported by the National Institutes of Health: National Institute of Environmental Health Sciences award number R15ES24593 and National Institute of General Medical Sciences award number P20GM103423 (an Institutional Development Award). University of Maine funding that additionally supported this work includes a UMaine Medicine Seed Grant, a Charlie Slavin Research Grant, Frederick Radke Undergraduate Research Fellowships, Maine Top Scholar research supply funds, and the Center for Undergraduate Research.

TABLE OF CONTENTS

ACKNOWLEDGEMENTS..... iii

LIST OF TABLES..... viii

LIST OF FIGURES.....ix

LIST OF ABBREVIATIONS..... xi

Chapter

1. INTRODUCTION.....1

2. METHODS.....9

2.1. Chemicals and reagents.....9

2.2. Cell culture.....9

2.3. Fluorescence photoactivation localization microscopy (FPALM) imaging and processing.....10

2.4. FPALM mitochondrial analysis.....10

2.5. Degranulation assay.....11

2.6. DiSC3(5) fluorescence interference assay.....11

2.7. Plasma membrane potential and cytosolic pH Assays in RBL-2H3 mast cells.....11

2.8. Plasma membrane potential assay in Jurkat T Cells.....12

2.9. Confocal microscopy.....13

2.10. Manual image analysis.....13

2.11. Automated image analysis.....14

2.12. Analysis of triclosan effects on ArcLight-A242 fluorescence intensity as a function of initial ArcLight-A242 expression Level.....15

2.13. Apparent plasma membrane potential percentage decrease calculations 15
2.14. TCS cytotoxicity on Jurkat cells 16
2.15. Cytosolic Ca^{2+}assay 17
2.16. Statistical analyses 18
3. RESULTS 19
3.1. Triclosan increases mitochondrial volume and surface area in RBL-2H3 mast cells: Indicators of inhibited mitochondrial membrane potential 19
3.2. Plasma membrane potential depolarizer gramicidin potently inhibits the degranulation of RBL-2H3 mast cells 20
3.3 Gramicidin and triclosan depress ArcLight-A242 fluorescence in RBL-2H3 mast cells 23
3.4 Non-cytotoxic doses of triclosan depress ArcLight-A242 fluorescence in Jurkat T cells 28
3.5. Triclosan does not depress the fluorescence of the genetically encoded voltage indicator ASAP2 in RBL-2H3 mast cells 30
3.6. Triclosan depresses fluorescence of a plasma membrane-targeted pHlourin in RBL-mast cells, indicating triclosan reduction of cytosolic pH 31
3.7. TCS inhibits cytosolic Ca^{2+} response to anti-T cell receptor stimulation in Jurkat T cells 33
4. DISCUSSION 35
REFERENCES 49
APPENDIX A: SUPPLEMENTARY INFORMATION TO CHAPTER 2 & 3 66
APPENDIX B: DIMETHYL SULFOXIDE EFFECTS ON GRAMICIDIN INHIBITION OF PLASMA MEMBRANE POTENTIAL 72

APPENDIX C: SUPPLEMENTARY INFORMATION TO CHAPTER 3 74

APPENDIX D: CYTOSOLIC CALCIUM OSCILLATIONS IN JURKAT T CELLS 75

APPENDIX E: OTHER CYTOSOLIC PH INDICATORS 78

APPENDIX F: CYTOTOXIC EFFECTS OF CETYLPYRIDINIUM CHLORIDE IN NIH-3T3 CELLS 79

BIOGRAPHY OF THE AUTHOR 80

LIST OF TABLES

Table 4.1 Summary of estimated changes in cytosolic pH following TCS exposure…….....40

LIST OF FIGURES

Figure 3.1. Triclosan effects on mitochondrial volume and surface area in RBL mast cells……20

Figure 3.2. Relative degranulation response of antigen-stimulated RBL mast cells exposed to micromolar doses of canonical plasma membrane depolarizer gramicidin.....22

Figure 3.3. Triclosan and gramicidin effects on fluorescence of ArcLight-A242 in RBL mast cells 24

Figure 3.4. Effect of cellular expression level of ArcLight-A242 on TCS inhibition of ArcLight-A242 fluorescence.....26

Figure 3.5. Triclosan and gramicidin apparent effects on plasma membrane potential (PMP) of RBL mast cells 27

Figure 3.6. Triclosan effects on fluorescence of ArcLight-A242 in human Jurkat T cells, triclosan apparent effects on Jurkat plasma membrane potential (PMP), and cytotoxicity determination 29

Figure 3.7. Triclosan effects on fluorescence of ASAP2 in RBL mast cells.....31

Figure 3.8. Triclosan effects on fluorescence of Lyn-tailed mCherry-SuperEcliptic (SE) pHluorin in RBL mast cells.....32

Figure 3.9. Triclosan effects on cytosolic Ca^{2+} levels as activated by anti-T Cell Receptor (TCR) antibody in Jurkat T cells 34

Figure 4.1 Relationship between mitochondrial surface area and volume.....36

Figure 4.2. Schematic diagram of TCS effects on mast cell degranulation through CRAC channel inhibition 47

Figure A.3. Triclosan effects on the fluorescence of ArcLight-A242 in RBL-2H3 mast cells when measured through automated image analysis 67
Figure A.4. Production, screening and fluorescence measurement of ArcLight-A242 RBL stably-transfected clones 68
Figure A.5. Widefield images of GCaMP6-transfected Jurkat T cells 71
Figure B.1. Effects of DMSO vehicle on gramicidin's ability to decrease Arclight fluorescence in RBL mast cells 72
Figure B.2. Effects of DMSO vehicle on Arclight fluorescence 73
Figure C.1. Effects of cellular expression level of ArcLight-A242 on TCS inhibition of ArcLight-A242 fluorescence in human Jurkat T cells 74
Figure D.1. Cytosolic Ca^{2+} levels as activated by anti-T Cell Receptor (TCR) antibody in individual Jurkat T Cells 75
Figure E.1 Transfection of cytosolic pH marker pME-pHluorin2 into RBL mast cells 78
Figure F.1 Cytotoxic effects of cetylpyridinium chloride (CPC) on NIH-3T3 cells 79

LIST OF ABBREVIATIONS

Ag	antigen
APC	antigen presenting cell
ATP	adenosine triphosphate
AUC	area under the curve
BSA	bovine serum albumin
BT	Tyrodes-bovine serum albumin
CCCP	carbonyl cyanide 3-chlorophenylhydrazone
CRAC	Ca^{2+} release-activated Ca^{2+}
DMSO	dimethyl sulfoxide
ER	endoplasmic reticulum
ETC	electron transport chain
FCCP	carbonyl cyanide-p-trifluoromethoxyphenylhydrazone;
FPALM	fluorescence photoactivation localization microscopy
GEVI	genetically encoded voltage indicator
IgE	immunoglobulin E
IP_3	inositol 1,4,5-trisphosphate
LDH	lactate dehydrogenase
MMP	mitochondrial membrane potential
PBS	phosphate buffered saline
PIP_2	phosphatidylinositol 4,5-bisphosphate
PLCγ	phospholipase C gamma
PLD	phospholipase D
PMP	plasma membrane potential
PSF	point spread function
RBL	rat basophilic leukemia cells, clone 2H3
ROI	region of interest
ROS	reactive oxygen species
SEM	standard error of the mean;
SOCE	store operated Ca^{2+} entry
STIM-1	stromal interaction molecule 1
TCR	T-cell receptor
TCS	Triclosan
TM	Transmembrane domain

CHAPTER 1

INTRODUCTION

Triclosan (TCS) is a formerly widespread antimicrobial agent: it was estimated that 75% of the US population in 2008 was exposed to TCS (Calafat *et al.*, 2008). Recently, the U.S. Food and Drug Administration effectively banned TCS from hand soaps in 2016 (Kux, 2016b), from hospital products in 2017 (Kux, 2017), and from over-the-counter hand sanitizers in 2019 (Gottlieb, 2019). TCS was also removed by the Colgate-Palmolive company from its top-selling toothpaste product (Kary, 2019) in 2019. Despite these stoppages, TCS remains in some antibacterial household products that are not regulated by the FDA and in a few remaining personal care products (www.ewg.org). TCS is readily absorbed into the skin (Queckenberg *et al.*, 2010) and oral mucosa (Gilbert, 1987) where it remains for a significant time prior to metabolism and clearance (Moss *et al.*, 2000), thus allowing for a constant chronic exposure upon periodic re-exposure. In this study, non-cytotoxic, micromolar TCS doses, that model human exposure levels to TCS following personal care product application (Weatherly and Gosse, 2017; Weatherly *et al.*, 2018), are utilized. Added to consumer products for its antimicrobial properties, TCS, ironically, inhibits the functioning of mammalian immune cells whose physiological purpose is to fight microbial infections (Udoji *et al.*, 2010; Palmer *et al.*, 2012; Hurd-Brown *et al.*, 2013).

Clinically, TCS is used for its antimicrobial (Daoud *et al.*, 2014) and anti-gingival properties (Rover and Leu-Wai-See, 2014). Additionally, previous studies provided evidence that TCS could potentially be used to treat atopic dermatitis (Sporik and Kemp, 1997; Tan *et al.*, 2010). Despite these positive clinical effects, within the past few years a panoply of triclosan

epidemiology studies have emerged, reporting various adverse TCS health effects (Weatherly and Gosse, 2017). Adverse TCS-linked effects on the reproductive system include increased spontaneous abortion rate (Wang *et al.*, 2015), abnormal sperm morphology (Jurewicz *et al.*, 2018; Zamkowska *et al.*, 2018), and decreased fecundity (Vélez *et al.*, 2015; Zhu *et al.*, 2019). Additionally, newborn infants' weight, length, and head circumference decreased due to TCS exposure (Etzel *et al.*, 2017). Cognitive effects have also been observed; TCS has been linked to lower cognitive test scores in children (Jackson-Browne *et al.*, 2018) and to higher behavior problem scores in 8-year old boys (Jackson-Browne *et al.*, 2019). TCS causes metabolic effects including decreased BMI (Li et al., 2015), increased risk of gestational diabetes (Ouyang *et al.*, 2018), changes in thyroid hormone levels in blood (Koeppe *et al.*, 2013; Wang *et al.*, 2017) and increased risk of type 2 diabetes in women (Xie *et al.*, 2020). Triclosan exposure is also associated with decreased bone mass density and increased osteoporosis (Cai *et al.*, 2019). Additionally, allergic rhinitis has been associated with TCS exposure (Kim and Kim, 2019). However, the cellular and molecular mechanisms underlying these epidemiological observations are not fully understood. Triclosan inhibition of mast cells (Palmer *et al.*, 2012; Weatherly *et al.*, 2013) and mitochondria (Ajao *et al.*, 2015; Shim *et al.*, 2016; Weatherly *et al.*, 2016; Weatherly *et al.*, 2018; Weatherly *et al.*, 2020), in human cells (Weatherly *et al.*, 2016) and in other species, may be related to these human health effects.

One of the underlying mechanisms of adverse human health effects caused by TCS may be its mitochondrial toxicity. An uncoupler due to its ionizable proton (Ajao *et al.*, 2015; Weatherly *et al.*, 2016), triclosan inhibits adenosine triphosphate (ATP) production and increases oxygen consumption rate in multiple cell types (Weatherly *et al.*, 2016) and in live zebrafish (Shim *et al.*, 2016). Additionally, TCS deflates mitochondrial membrane potential (MMP),

thwarts mitochondrial translocation and Ca^{2+} dynamics, and induces mitochondrial fission and deformation (as assessed in two-dimensional [2D], super-resolution, live-cell microscopy (Weatherly *et al.*, 2018). Mitochondria play a role in cytosolic and ER Ca^{2+} uptake that supports Ca^{2+} homeostasis in cells, which are important mechanisms needed in maintaining mast cell functions (Takekawa *et al.*, 2012; Furuno *et al.*, 2015). These TCS effects on MMP and mitochondrial morphology have been recapitulated in an *in vivo* mouse study (Weatherly *et al.*, 2020). Critically, mitochondrial toxicity by TCS has been directly connected to its instigation of inflammation and immunotoxicity: TCS increases Drp1 and decreases Opa1 expression levels, effects which both increase mitochondrial fission and activate the NLRP3 inflammasome (Weatherly *et al.*, 2020).

Separate from its mitochondrial toxicity, TCS disrupts other cellular signal transduction processes, such as Ca^{2+} mobilization and cytoskeletal remodeling, which are shared by numerous cell types (Weatherly *et al.*, 2018). For example, TCS disrupts the functioning of the immunological/neurological cell type mast cells; TCS mitotoxicity does not explain this inhibition (Weatherly *et al.*, 2018). Mast cells are found in a large variety of tissues (Dvorak, 1986; Theoharides and Sant, 1991; Farrell *et al.*, 1995; Blank *et al.*, 2007) and are involved in defense against parasites (Metcalfe *et al.*, 1997), bacteria (Johnzon *et al.*, 2016), and cancer (Hempel *et al.*, 2017). Mast cell dysfunction is associated with neurological diseases (Silver and Curley, 2013; Girolamo *et al.*, 2017) such as multiple sclerosis (Elieh-Ali-Komi and Cao, 2017). Of course, mast cells are also major effector cells of allergy and asthma (Galli *et al.*, 2005), and previous clinical reports of atopic disorder alleviation by TCS, noted above (Sporik and Kemp, 1997; Tan *et al.*, 2010), align with our findings of mast cell inhibition by TCS (Palmer *et al.*, 2012).

Mast cells undergo degranulation, the release of bioactive mediators such as histamine and serotonin, in a process that begins with multivalent antigen (Ag) mediated cross-linking of immunoglobulin E (IgE)-primed FcεRI receptors on the cell surface. This binding initiates a phosphorylation cascade in which phospholipase C gamma (PLCγ) is activated (Kinet, 1999). PLCγ subsequently cleaves phosphatidylinositol 4,5-bisphosphate (PIP_2) into diacylglycerol (DAG) and inositol 1,4,5-trisphosphate (IP_3). The latter is then able to bind to its receptor on the endoplasmic reticulum (ER) membrane and initiate the release of ER Ca^{2+} stores into the cytosol (Berridge, 1993). Reduced ER Ca^{2+} concentration results in altered conformation of ER protein STIM1, causing it to bind to and change the conformation of the Orai1 subunit of the Ca^{2+} release-activated Ca^{2+} (CRAC) channel, opening it to a flood of external Ca^{2+} flowing into the cytosol (Vig *et al.*, 2006; Hogan *et al.*, 2010); this process is termed store-operated Ca^{2+} entry, or SOCE (Putney, 1986). SOCE is required for mast cell degranulation (as reviewed in (Holowka *et al.*, 2012) because increased cytosolic Ca^{2+} levels allow for events required for the movement of granules to the plasma membrane for exocytosis, such as protein kinase C (PKC) activation (Ozawa *et al.*, 1993), phospholipase D (PLD) activation (Chahdi *et al.*, 2002), and microtubule polymerization (Guo *et al.*, 1998; Smith *et al.*, 2003).

These signaling processes are important in a variety of cell types, including in the immune system and brain. SOCE mechanisms are largely conserved across cell types (Prakriya and Lewis, 2015). For example, T-cell signaling (Marano *et al.*, 1993; Trebak and Kinet, 2019) also begins with T-cell receptor (TCR) cross-linking, as with FcεRI. In T-cells (part of the adaptive immune system) *in vivo*, this crosslinking is primarily done by an antigen presenting cell (APCs; innate immune cells such as macrophage or a dendritic cells), presenting antigen on

the major histocompatibility complex (Punt *et al.*, 2019). The TCR/APC interaction can be emulated *in vitro* through the use of an anti-TCR antibody (Marano *et al.*, 1993). Such cross-linking leads to PLCγ activation and subsequent generation of IP_3 and SOCE, via the same process outlined above for mast cells. The subsequent increase in cytosolic Ca^{2+} concentration allows for calmodulin/calcineurin binding and subsequent activation of the nuclear factor of activated T-cells (Punt *et al.*, 2019; Trebak and Kinet, 2019), an important Ca^{2+}-dependent transcription factor. Thus, signaling upstream of SOCE is very similar between mast cells and T-cells; whereas signaling downstream of SOCE is largely different between mast cells and T-cells. While TCS is known to interfere with bodily distribution of T cells (Anderson *et al.*, 2016), cytokine production (Barros *et al.*, 2010; Marshall *et al.*, 2015; Anderson *et al.*, 2016; Marshall *et al.*, 2017), and expression of calcium-binding biomarkers of inflammation (Marshall *et al.*, 2017), triclosan effects on intracellular signal transduction, functional outcomes, and SOCE within T cells have not yet been examined.

Triclosan disrupts mast cell function by strongly inhibiting Ag-stimulated Ca^{2+} influx into the cytosol via the CRAC channels (Weatherly *et al.*, 2018). This depressed cytosolic Ca^{2+} concentration leads, as expected, to inhibition of downstream events, such as reduced PLD activity (Shim *et al.*, 2019) and microtubule polymerization (Weatherly *et al.*, 2018). Thus, inhibition of SOCE by TCS explains its inhibition of mast cell function. The question remains: how does TCS inhibit Ca^{2+} entry through CRAC channels?

One explanation could be TCS disruption of any of the upstream signaling events leading to SOCE: FcεRI crosslinking, any link in the phosphorylation cascade, PIP_2 signaling function, or IP_3 binding to its ER membrane receptor. However, TCS does not hinder Ca^{2+} efflux from the

ER (Weatherly *et al.*, 2018) and does not seriously interfere with PIP_2 (Shim *et al.*, 2019)—evidence that TCS does not inhibit any of these events upstream of ER Ca^{2+} release.

Because TCS does not hamper the signaling events culminating in ER Ca^{2+} release, an alternative mechanism underlies TCS inhibition of CRAC channel Ca^{2+} entry. Chemical depolarization of plasma membrane potential (PMP) reduces Ca^{2+} entry into the cytosol of mast cells (Mohr and Fewtrell, 1987a) and also of T cells (Sarkadi *et al.*, 1990). Integrity of PMP is important for SOCE due to its contribution to the free energy, $\Delta G_{transport}$, available to import Ca^{2+} down its electrochemical gradient into the cytoplasm. In this study, we hypothesized that TCS, as a proton ionophore (Weatherly *et al.*, 2016), inhibits Ca^{2+} influx by depolarizing PMP similarly to how TCS deflates membrane potential of mitochondria (Weatherly *et al.*, 2018) and of artificial bilayers (Popova *et al.*, 2018)—by acting as a "Trojan horse" to provide safe passage for protons through lipid membranes.

The driving force for Ca^{2+} influx through the CRAC channel is calculated as (Nelson and Cox, 2017)

$$\Delta G_{Transport} = RTln\left(\frac{C_2}{C_1}\right) + nZF\Delta\Psi$$

Using physiological temperature of 310K, the gas and Faraday's constants, the number of charges on the transported ion (n=2), the sign of the charge of the transported ion (Z=+), resting PMP $\Delta\Psi$ of -82.5 mV (Lindau and Fernandez, 1986; Wischmeyer *et al.*, 1995), C_1 = extracellular Ca^{2+} concentration in the buffer (1.8 mM), and C_2 = average cytosolic Ca^{2+} concentration in an Ag-stimulated mast cell (1 μM) (Millard *et al.*, 1988; Chandra *et al.*, 1994), the driving force (Gibbs free energy) for Ca^{2+} influx through open CRAC channels is the highly exergonic value -35 kJ/mol. If TCS were to completely depolarize the mast cell PMP, the term $nZF\Delta\Psi$ would collapse to zero, the driving force behind SOCE would be reduced ~45%, to -19

kJ/mol, and, hence, 45% less Ca^{2+} would flood into the cell. In fact, this PMP-knockout-predicted ~45% reduction in integrated Ca^{2+} influx was observed in mast cells following 20 μM TCS exposure (Weatherly *et al.*, 2018).

Thus, in this study, the first aim was to measure TCS effects on PMP in mast cells. The mast cell model rat basophilic leukemia, clone 2H3 (RBL), which are functionally similar to mature human mast cells, rodent mucosal mast cells, and basophils (Fewtrell *et al.*, 1979; Metzger *et al.*, 1982; Seldin *et al.*, 1985; Metcalfe *et al.*, 1997; Abramson and Pecht, 2007; Lee *et al.*, 2012), was used. RBL cells are effective for toxicological studies due to their ability to respond to exogenous agents in a similar fashion as primary bone-marrow derived mast cells (Zaitsu *et al.*, 2007; Thrasher *et al.*, 2013; Alsaleh *et al.*, 2016).

Conventionally, PMP is measured through the use of patch clamping or of voltage-sensitive fluorescent organic dyes. However, traditional patch clamping is a low-throughput process. Also, TCS is a chemical quencher of many unprotected fluorescent chromophores (such as those found in organic voltage sensitive dyes) (Weatherly, 2017). Thus, genetically encoded voltage indicators (GEVIs), reporter protein constructs with a β-barrel protein structure that protects the internal fluorophore from TCS fluorescence interference (Weatherly, 2017; Weatherly *et al.*, 2018) were used. Targeted to the plasma membrane, GEVIs communicate changes in PMP through changes in fluorescence intensity. To our knowledge, this study represents the first use of a GEVI in an immune cell model or in the field of toxicology.

An additional novel use of a biophysical technique in toxicology, three-dimensional (3D) Fluorescence Photoactivation Localization Microscopy (FPALM) super-resolution microscopy was also employed to detail TCS effects, via membrane depolarization, on mitochondrial morphology in mast cells (Parent and Hess, 2019). Conventional light microscopy, including

widefield and confocal imaging, cannot resolve objects that are less than ~250 nm apart, due to the diffraction limit, but FPALM breaks this diffraction limit (Hess *et al.*, 2006). These 3D studies augment, by providing information on mitochondrial volume and surface area, previous 2D work showing that TCS disrupts mitochondrial nanostructure, causing "donut" shapes or fragmentation (Weatherly *et al.*, 2018).

In this study, we test the hypothesis that TCS inhibits mast cell function by depolarizing the plasma membrane. However, careful experimentation with two GEVI constructs, which function via disparate molecular machinery, indicate a wholly different mechanism of TCS action: cytoplasmic acidification. Furthermore, TCS replicates this mechanism of action and abrogation of function in another immune cell type, T cells.

CHAPTER 2

METHODS

2.1 Chemicals and reagents

Triclosan (TCS; 99% purity; Sigma-Aldrich) was prepared in BT (Tyrodes buffer containing bovine serum albumin [BSA]) without use of organic solvent (Weatherly *et al.*, 2013) and diluted to deliver non-cytotoxic concentrations (Palmer *et al.*, 2012) checked by UV-Vis spectrophotometry (Weatherly *et al.*, 2013). Gramicidin (Sigma- Aldrich) was dissolved in 100% DMSO (Sigma-Aldrich) and diluted with BT.

2.2 Cell culture

RBL-2H3 mast cells were cultured as in (Hutchinson *et al.*, 2011).

Human Jurkat T cells, clone E6-1, were obtained from ATCC and maintained in suspension in phenol red-containing RPMI-1640 medium (ATCC) supplemented with 10% fetal bovine serum (Atlanta Biologics) and 100 U/ml penicillin-100 µg/ml streptomycin (Sigma-Aldrich). Cells were passaged once a week with thorough trituration technique to break up clumps, seeded at 35,000 cells/mL (for 6-7 days until harvest) to 125,000 cells/mL (for 3 days), and grown at 37°C and 5% CO_2. Supplement fresh media was added after 3 days in culture. These culturing conditions resulted in maximal cell density of 1-2 million cells/mL.

2.3 Fluorescence photoactivation localization microscopy (FPALM) imaging and processing

Three-dimensional FPALM mitochondrial imaging was performed as in (Parent and Hess, 2019). RBL cells were transfected with an expression vector for Dendra2-Tom20 (Weatherly *et al.*, 2018) using an Amaxa transfection kit (Lonza), then plated in μ-Slide 8-well plates with polymer coverslip (ibidi) at 100,000 cells/well in 200 μL/well phenol red-free RBL media. The next day, cells were exposed to 20 μM TCS or BT for 1 hour and fixed with 4% paraformaldehyde (Sigma Aldrich) before imaging. Imaging was performed using a 558 nm laser (Crystalaser) for Dendra2-Tom20 excitation, and fluorescence was captured using an Olympus IX-71 microscope with 60X 1.45NA oil lens, 2X telescope, and an EMCCD camera (Andor iXon DU-897 #BV). Custom MATLAB analysis software was used to obtain localized data points (Hess *et al.*, 2006; Gudheti *et al.*, 2013; Curthoys *et al.*, 2019); details of microscopy are in Appendix A.1 and A2.

2.4 FPALM mitochondrial analysis

In MATLAB, raw data was localized first by fitting each Point Spread Function (PSF) to a two-dimensional (2D) Gaussian, which was then drift corrected. After drift correction, following the methods in (Huang *et al.*, 2008; Parent and Hess, 2019), the z-coordinate of each localized point was obtained from the measured calibration curve connecting the x- and y-widths of the PSF as a function of z- position. After obtaining the z-position for each localized point, the data set was processed through another custom MATLAB script for cluster identification, which compares the distances between each localization and all nearby localizations: localizations that lie within d_{max} (75 nm) of each other are considered to be in the

same cluster. Clusters with a minimum number of 50 localizations were analyzed further. The nearest-neighbor single linkage cluster analysis (SLCA) method (Sneath, 1957; Gudheti *et al.*, 2013) used here has been extended to three dimensions (Parent and Hess, 2019). Each cluster is then analyzed using the MATLAB convex hull and alpha shape functions, in order to quantify the local mean curvature for all localizations within an individual mitochondrion. Histograms and averages of the curvature, area, and volume of the convex and alpha hulls are then determined.

2.5 Degranulation assay

Degranulation assays were performed as in (Weatherly *et al.*, 2013), adapted for use with gramicidin in 0.003% DMSO vehicle.

2.6 DiSC$_3$(5) fluorescence interference assay

Triclosan effects on DiSC$_3$(5) (TCI America) organic voltage sensitive dye fluorescence were assayed. The dye was dissolved in 100% DMSO. In a 96 well black bottom plate (Greiner), DisC$_3$5 dye and TCS were mixed to achieve a final dye concentration of 1.02 μM in 0.01% final DMSO percentage, with various TCS concentrations (1-15 μM) in BT. The mixture was allowed to equilibrate for 10 min at 37°C. Fluorescence measurements were taken using a microplate reader (Synergy 2, Biotek) with 530 ± 20 nm excitation and 645 ± 15 nm emission.

2.7 Plasma membrane potential and cytosolic pH assays in RBL-2H3 mast cells

In order to measure changes in plasma membrane potential, RBL cells were transfected with genetically-encoded voltage indicator (GEVI) protein construct ArcLight-A242 (a gift from

Vincent Pieribone; Addgene plasmid # 36857; http://n2t.net/addgene:36857; RRID:Addgene_36857) (Jin *et al.*, 2012) or ASAP2 (pcDNA3.1/Puro-CAG-ASAP2s was a gift from Francois St-Pierre; Addgene plasmid # 101274; http://n2t.net/addgene:101274; RRID:Addgene_101274) (Chamberland *et al.*, 2017). To investigate TCS effects on cytosolic pH, RBL cells were transfected with plasma membrane-targeted Lyn-tailed mCherry-SuperEcliptic (SE) pHluorin protein construct (Lyn-tailed mCherry-SEpHlourin was a gift from Sergio Grinstein; Addgene plasmid # 32002; http://n2t.net/addgene:32002; RRID:Addgene_32002) (Koivusalo *et al.*, 2010). RBL cells were transiently transfected with ArcLight A242, ASAP2, or Lyn-tailed mCherry-SuperEcliptic (SE) pHluorin through electroporation using RBL-specific Amaxa Nucleofector transfection kit T (Lonza), then plated in 8-well plates (ibidi) at ~150,000 cells/well in 200 µL/well phenol red-free RBL media. Cells were grown for 16-24 hrs at 37ºC/ 5% CO_2. Before imaging, cells were washed with BT and the media was replaced with 200 µL BT. After the initial, untreated, image was taken, cells were treated with 200 µL of either BT (for control) or various 2X concentrations of TCS or gramicidin, depending on the experiment. See "Confocal Microscopy" below for imaging details.

2.8 Plasma membrane potential assay in Jurkat T cells

Ibidi 8-well plates were coated with 150 µL of human fibronectin (VWR) prepared at 166 µg/ml in phosphate buffered saline (PBS) (Lonza) (Wang *et al.*, 2019) overnight in the tissue culture incubator (37ºC/ 5% CO_2); these wells were washed the next day with 200 µL PBS/well before use. Jurkat cells were transiently transfected with ArcLight-A242 through electroporation using Jurkat-specific Amaxa Nucleofector transfection kit T (Lonza), then plated in the

fibronectin pre-coated plates at ~1million cells/well in 300 µL phenol red-free Jurkat media. Cells were grown for 16-24 hours at 37ºC/ 5% CO_2. Next day, cell media was removed carefully with a transfer pipette to avoid cell detachment and replaced with 200 µL control BT before imaging. After the initial, untreated, image was taken, cells were treated with 200 µL of either additional BT (for control) or various 2X concentrations of TCS. See "Confocal Microscopy" below for imaging details.

2.9 Confocal microcopy

For plasma membrane potential and cytosolic pH assays, an Olympus FV-1000 confocal microscope, with an Olympus IX-81 inverted microscope and a 30 milliwatt multi-argon laser, was used to collect images. ArcLight-A242 and ASAP2 plasmid-transfected cells were imaged using an oil immersion 100x objective with NA 1.4 and 488 nm excitation, 505-605 nm band pass emission filter. Lyn tailed mCherry-SEpHluorin transfected cells were imaged using oil immersion 60x objective with NA 1.4 and 488 nm excitation, 505-525 nm emission filter. All images were taken at 37°C using ibidi plate heating system.

2.10 Manual image analysis

All image-analysis figures in this paper were generated with this manual method except for Figure 3.8 and Appendix Figure A.3, which were analyzed with the automated image analysis procedure noted below. Confocal microscopy images of RBL and Jurkat cells transfected with ArcLight and ASAP2 were analyzed manually using Fiji ImageJ software (NIH). Well-transfected cells (i.e. visible expression of reporter and well-targeted to the plasma membrane) were identified and a Region of Interest (ROI) was drawn on the plasma membrane

using the free-hand tool. The area of the ROI (in units of square pixels), integrated density (= sum of fluorescence intensity values of all pixels in the ROI), mean intensity (= integrated density divided by area of the ROI), and length of the ROI were subsequently measured at various specified time points before and after treatment.

Mean background fluorescence intensity (=integrated density of ROI divided by area of ROI) for a field of view, was obtained by either drawing a square shape ROI in the cytoplasmic region of transfected cells or by drawing an ROI around the plasma membrane of untransfected cells. Background mean fluorescence intensity obtained through either of these methods was subtracted from mean ArcLight fluorescence intensity of cells present in that field of view, and the resulting value at each time point was then normalized to (divided by) its own 0 min timepoint value of mean intensity. Both of these background subtraction methods resulted in similar ArcLight fluorescence changes due to 20 μM TCS (data not shown). Photobleaching or drifting effect during imaging was calculated from BT-treated (control) cells by calculating a change in fluorescence values from 0 min. This change value was added/subtracted back to the treatment groups to account for these non-treatment effects and thus allowing measure of the true effect of a drug. Normalized values from multiple cells were averaged and used to generate line plots.

2.11 Automated image analysis

In FIJI image J, individual images at different time points (0, 2, 5, 7, and 15 min) were converted to 8-bit stack. Background fluorescence was subtracted from the stack using pseudo flatfield correction. Next, by applying threshold, binary masks of the entire cell and only cytosol were created. Both of these masks were applied to transfected cells to obtain area of the ROI,

integrated density, and mean intensity values. To find the area of the ROI, mean intensity and integrated density of plasma membrane, values of cytosol were subtracted from the area of the ROI and integrated density of whole cell. The calculated integrated density was divided by the calculated area of ROI. This will give mean fluorescence intensity of the plasma membrane. Mean intensity at different time points of an individual cell was normalized to (divided by) its own 0 min time point value of mean intensity. Fluorescence was adjusted for drifting or photobleaching as described in "Manual Image Analysis" methods above. This automated method was utilized to generate Figure 3.8 and Appendix Figure A.3.

2.12 Analysis of triclosan effects on ArcLight-A242 fluorescence intensity as a function of initial ArcLight-A242 expression level

Initial (0 min) mean plasma membrane fluorescence intensity of ArcLight for each individual cell was noted. Next, for each individual cell, the percentage drop in ArcLight fluorescence mean intensity incurred by 15 min exposure to 20 μM triclosan (or to control BT) was then plotted as a function of that cell's initial mean intensity of ArcLight (its expression level of the construct). Linear regression analysis was performed, and the slope of the best-fit line and R^2 value was determined for each plot.

2.13 Apparent plasma membrane potential percentage decrease calculation

Apparent PMP percentage decrease was calculated for the treatments, cell types, and GEVIs utilized in this study. Each normalized and photobleaching-/drift-corrected GEVI fluorescence value was subtracted from 1 to determine change in fluorescence due to treatment. This result was subsequently multiplied by its respective reporter's PMP to fluorescence change

ratio to calculate mV change as reported by each construct. For ArcLight-A242, this ratio is 100 mV for every 35% decrease in fluorescence (100 mV/0.35) (Jin *et al.*, 2012). For ASAP2, this ratio is 100 mV for every 39% decrease in fluorescence (100 mV/0.39) (Chamberland *et al.*, 2017). This change, in units of mV, was then divided by the resting PMP of the corresponding cell type, RBL mast cell (-82.5 mV is the average value from two patch-clamp studies (Lindau and Fernandez, 1986; Wischmeyer *et al.*, 1995)) or T cell (-60 mV)(Sarkadi *et al.*, 1990) to determine the (unitless) change in total resting cell PMP. Finally, this result was subsequently subtracted from 1 and multiplied by 100 to obtain the apparent PMP percentage.

2.14 TCS cytotoxicity on Jurkat cells

Trypan blue exclusion and lactate dehydrogenase (LDH) cytotoxicity assays were used to assess TCS cytotoxicity on Jurkat cells. In the trypan blue exclusion assay, 1 million cells were plated into each of 3 wells of a 24-well, flat-bottom cell culture plate (Costar) for TCS (Sigma) treatment and 3 wells for the control. Immediately after plating, BT and 2X TCS doses were added to respective wells. Next, cells were incubated for 30 minutes at 37°C/5% CO_2. After the incubation, a small sample was taken from each well and mixed 1:1 with trypan blue dye (0.4%, Lonza) evenly. Cells were counted using a hemocytometer for viability and TCS-treated cells were normalized to the control. LDH cytotoxicity methods were those of Hutchinson *et al*., 2011 using a cytotoxicity detection kit (Roche). However, the lysis solution was added to the "high control" in the final 15 minutes of the 1-hour TCS exposure instead of an additional 15 minutes after the 1-hour TCS exposure (Palmer *et al.*, 2012).

2.15 Cytosolic Ca^{2+} assay

Prior to performing Ca^{2+} assays, widefield fluorescence microscopy was used to assess transfection efficiency of GCaMP6 Ca^{2+} reporter construct in Jurkat T cells, and Ca^{2+} assays were performed only on samples of highly-transfected cells. First, 8-well ibidi plates were coated with 150 µL/well fibronectin (166 µg/ml) prepared in PBS and incubated overnight in tissue culture incubator. The next day, Jurkat T cells were transfected with pGP-CMV-GCaMP6f (a gift from Douglas Kim & GENIE Project; Addgene # 40755; http://n2t.net/addgene:40755; RRID: Addgene_40755) (Chen *et al.*, 2013) using Jurkat specific Amaxa Nucleofector transfection kit T (Lonza). The electroporated cells were plated in phenol red-free Jurkat cell media at ~1 million cells/well with phenol red-free media in the fibronectin pre-coated 8-well ibidi plates. Cells were grown for 16-24 hours at 37ºC/ 5% CO_2. The next day, cell media was removed carefully with a transfer pipette to avoid cell detachment and replaced with 200 µL BT, and images were taken with a wide-field IX83 (Olympus, Waltham MA) microscope with a Prime 95B CMOS Camera (Photometrics) and HLD117 stage (Prior Scientific) controlled by a Proscan III. Fluorescence excitation was provided by an Xcite 120 LEDBoost (Excelitas). Images were taken at 60x (Olympus-APON-60X-TIRF objective) using standard excitation and emission filters for GFP (Semrock). The microscope is controlled by CellSens software v1.18 (Olympus).

For assessment of Jurkat T cell cytosolic Ca^{2+} levels following anti-T cell receptor (anti-TCR) stimulation, a plate reader assay was performed similarly to that in (Weatherly *et al.*, 2018), with the following modifications. First, a 96-well, black-walled, clear-bottom plate (Grenier) was coated overnight with 50 µL/well fibronectin (166 µg/ml) prepared in PBS (Lonza). The next day, cells were transfected with the GCaMP6 construct as noted above and

plated in 200 µL/well phenol red-free media in the fibronectin pre-coated 96-well plate at 330,000 cells/well. Cells were cultured overnight at 37°C and in 5% CO_2. Next day, media was carefully aspirated from wells with a micropipette to avoid cell detachment, and cells were exposed to 100 µL/well 0.2 µg/ml (Holowka *et al.*, 2018) Anti-TCR OKT3 monoclonal antibody (Thermo Fisher Scientific) in combination with control BT or TCS treatments for 1 hour. Fluorescence was measured with 485 ± 10 nm excitation and 528 ± 10 nm emission during this 1 hour. Area under the curve was determined as per methods in Weatherly *et al*., 2018.

2.16 Statistical analyses

All analyses were performed in Graphpad Prism. In most figures, raw values for treatment groups were normalized to its appropriate untreated control. Biological replicates from at least three independent experiments were averaged, and standard error of the mean (SEM) was calculated across those independent experiments. Raw (non-normalized) values were analyzed for mitochondria swelling and LDH release experiments (Figures 3.1, 3.6D). One-way ANOVA followed by Tukey's *post-hoc* test (α=0.05) was used to determine the significance level of most experiments (Figures 3.2, 3.3B, 3.5, 3.6, 3.7B, 3.8, Appendix A.3 and A.4). The significance level of the FPALM mitochondrial volume and surface area were assessed using an unpaired one-tailed t-test (Figure 3.1). The significance level of the cytosolic Ca^{2+} level area under the curve (AUC) of Jurkat cells was assessed via paired t-test (Figure 3.9B). Significance is represented by ***p<0.001, **p<0.01, and *p<0.05.

CHAPTER 3

RESULTS

3.1 Triclosan increases mitochondrial volume and surface area in RBL-2H3 mast cells: Indicators of inhibited mitochondrial membrane potential

Previously, an organic dye fluorescence method (without imaging) revealed that TCS inhibits MMP (Weatherly *et al.*, 2018). To test this finding at the nanoscale, three-dimensional super-resolution FPALM imaging (Huang *et al.*, 2008; Parent and Hess, 2019) was employed to assess TCS effects on 3D mitochondrial morphology, changes in which are linked to inhibition of MMP (Guillery *et al.*, 2008; Giedt *et al.*, 2012; Weatherly *et al.*, 2018). RBL cells were transiently transfected with Dendra2-TOM20 (Weatherly *et al.*, 2018), a construct used to label the outer membrane of mitochondria. The next day, cells were exposed with TCS or BT control for 1 hour, then fixed using paraformaldehyde.

While the TCS effects on mitochondrial volume and surface area were not dramatic visually, they were statistically significant when analyzed quantitatively. Triclosan statistically significantly increases the mean volume, as calculated by the convex hull method, by 17% compared to control (Figure 3.1A). Also, triclosan increases the mean mitochondrial surface area, as calculated by the alpha shape method, by 19% (Figure 3.1B). Thus, TCS modulates the surface area and volume of individual mitochondria, as assessed with 3D FPALM super-resolution microscopy.

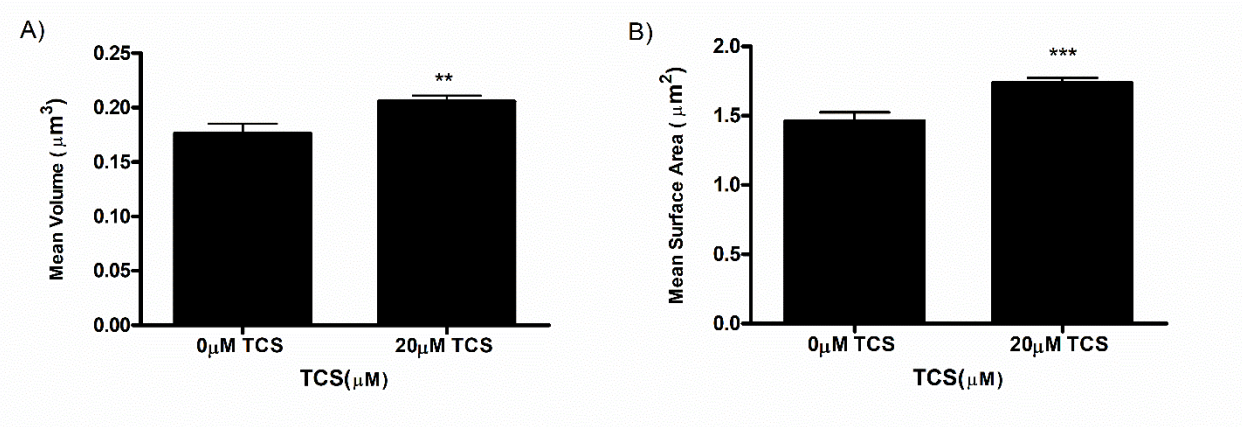

Figure 3.1. Triclosan effects on mitochondrial volume and surface area in RBL mast cells. Super-resolution FPALM 3D images of Dendra2-TOM20, which labels outer mitochondrial membranes, were processed through custom-built MATLAB code in which an algorithm identifies individual mitochondria. As detailed in Chapter 2, (A) average mitochondrial volume was calculated by the convex hull method, and (B) average mitochondrial surface area was calculated by the alpha shape method. Values presented are mean ± SEM for total of 62 cells in three independent experiments, where each independent experiment had 8-11 cells for each condition (0 vs. 20 μM triclosan). Statistically significant results are represented by **$p<0.01$ and ***$p<0.001$ as compared to control (0 μM TCS) for volume and surface area, respectively, as determined by unpaired t-test.

3.2 Plasma membrane potential depolarizer gramicidin potently inhibits the degranulation of RBL-2H3 mast cells

To determine the effects of the canonical plasma membrane depolarizer, gramicidin, on RBL mast cell degranulation, an adapted fluorescence-based β-hexosaminidase release assay (Weatherly *et al.*, 2013) was employed. A multivalent DNP (dinitrophenol)-BSA Ag was used to laterally crosslink IgE-bound FcεRI receptors, thus initiating an allergic/pro-inflammatory signal transduction that ends with the release of granules containing bioactive substances including β-hexosaminidase, which is monitored fluorometrically. Gramicidin depolarizes cells by forming an ion channel at the plasma membrane, allowing for free passage monovalent ions such as H^+, NH_4^+, K^+, Na^+, and Li^+ down their concentration and electrochemical gradients, and, thus, depolarizing the plasma membrane (Myers and Haydon, 1972; Mohr and Fewtrell, 1987b).

Figure 3.2A presents the results for IgE-sensitized RBL cells incubated for 1 h in Tyrodes—BSA (BT) buffer containing a 0.0004 μg/ml Ag dose, with gramicidin or DMSO vehicle. All tested gramicidin doses, as low as 0.1 μM, inhibit degranulation, reducing the response down to the same level as the spontaneous group (unstimulated with Ag). These data indicate a potent, plasma membrane depolarization-mediated inhibition of degranulation. A similar, but slightly less potent, gramicidin-induced depression of degranulation can be seen in the group treated with the higher Ag dose, 0.001 μg/ml Ag (Figure 3.2B). In this case, statistically significant inhibition of degranulation does not begin until 0.5 μM gramicidin and appears to proceed in a dose-responsive fashion. Such data coincide with the previously reported observation that pharmacologically induced inhibition of degranulation occurs at lower toxicant doses when cells are stimulated at a low level (0.0004 μg/ml Ag) than when stimulated at a high level (0.001 μg/ml Ag) (Palmer *et al.*, 2012).

A dose comparison study for gramicidin and TCS was performed as part of testing the hypothesis that TCS inhibits degranulation via PMP inhibition, by repeating the above experiments with TCS in place of gramicidin at equivalent antigen and DMSO concentrations. While DMSO is not needed/used here to dissolve the TCS, it was included to match the conditions of the gramicidin experiments. Statistically significant, dose-responsive inhibition of mast cell degranulation by TCS is reported in Figures 3.2C and 3.2D, beginning at 10 μM (Figure 3.2C). This observation recapitulates previously observed TCS-mediated inhibition of degranulation (Palmer *et al.*, 2012), but the presence of DMSO reduces its potency: 10 μM TCS inhibits 0.0004 μg/ml Ag-stimulated degranulation by about one-half in the absence of DMSO (Weatherly *et al.*, 2013) and only by about one-third in the presence of 0.003% DMSO (Figure 3.2C). Also, the TCS inhibitory effect lessens in the presence of higher Ag dose (0.001 μg/ml

Ag; Figure 3.2D), as noted with gramicidin Figure 3.2B. Overall, depolarizer-mediated inhibition of degranulation (Figure 3.2A and 3.2B) proceeds similarly as that of TCS, though gramicidin is more potent than TCS, especially in the presence of DMSO. The result strengthens the connection between PMP inhibition and degranulation inhibition.

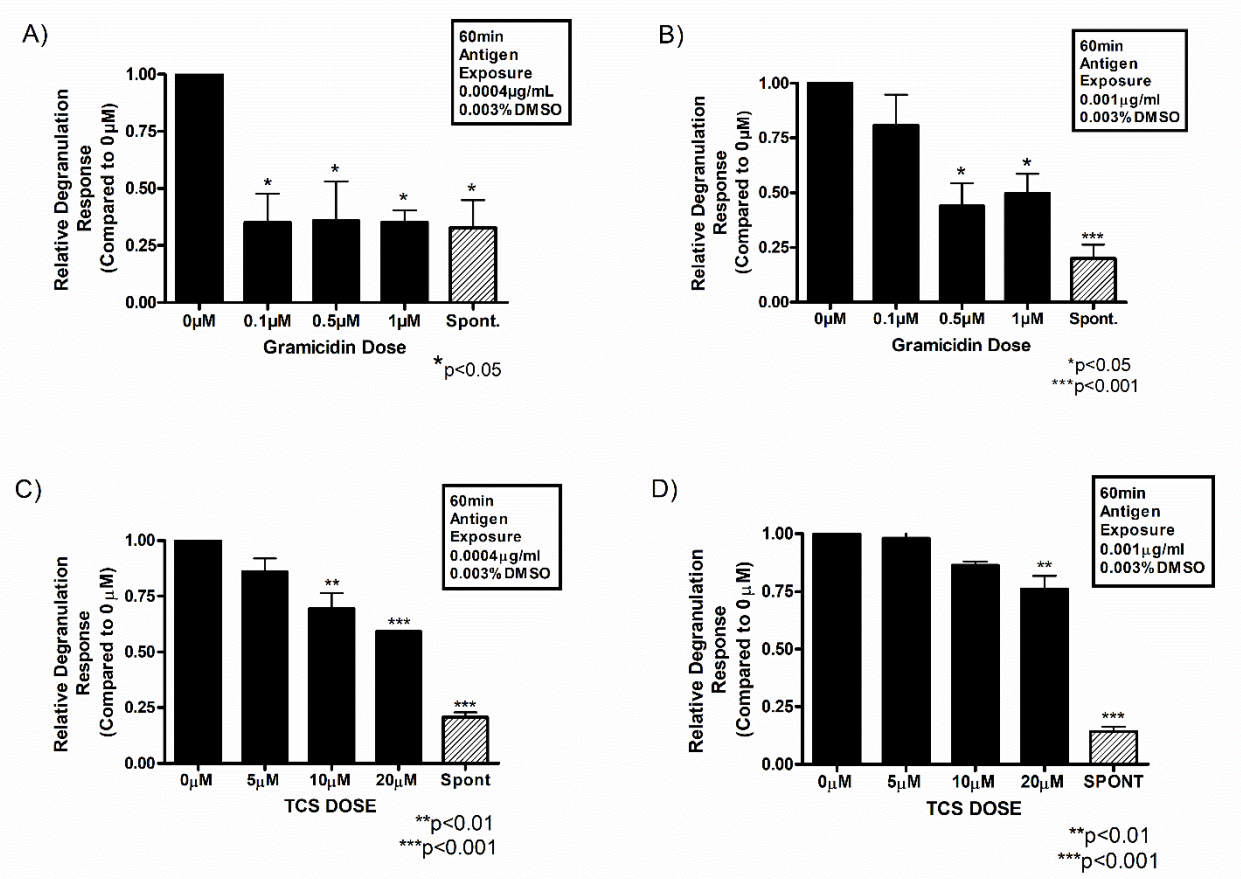

Figure 3.2 Relative degranulation response of antigen-stimulated RBL mast cells exposed to micromolar doses of the canonical plasma membrane depolarizer gramicidin (A and B) or to triclosan (C and D). IgE-sensitized cells were stimulated for 1 h with either 0.0004 µg mL^{-1} Ag (**A** and **C**) or 0.001 µg mL^{-1} Ag (**B** and **D**). All samples (**A** - **D**) contained 0.003% DMSO, which was the vehicle required for gramicidin dissolution. For spontaneous release ("Spont" on x-axes), cells were incubated for 1 h in BT with 0.003% DMSO (with no IgE, Ag, TCS, or gramicidin). Values represent the mean ± SEM of 3 independent experiments; three replicates per treatment type were used each experimental day. Statistically significant results, as compared to the appropriate control (0 µM TCS + DMSO vehicle) or (0 µM gramicidin + DMSO vehicle), are represented by *p < 0.05, **p < 0.01, ***p<0.001 as determined by one-way ANOVA followed by Tukey's post-hoc test.

3.3 Gramicidin and triclosan depress ArcLight-A242 fluorescence in RBL-2H3 mast cells.

Gramicidin, a known depolarizer of PMP, strongly inhibits degranulation (Figs. 3.2A and 2B), and TCS also reduces degranulation (Palmer *et al.*, 2012). Also, TCS depolarizes the MMP (Weatherly *et al.*, 2018) (Figure 3.1). Thus, we hypothesized that TCS also inhibits the PMP, as its underlying mechanism of degranulation inhibition. To do so, an organic voltage-sensitive fluorescent dye, $DiSC_3(5)$ was employed. However, when TCS (micromolar levels) and $DiSC_3(5)$ (1 μM) (Te Winkel *et al.*, 2016) are mixed together in the absence of cells, TCS chemically quenches the fluorescence of $DiSC_3(5)$ in a dose-response manner (data not shown); thus, $DiSC_3(5)$ cannot be used to accurately measure TCS effects on PMP. Triclosan quenching of unprotected fluorophores (such as those found in various voltage-sensitive, fluorescent organic dyes) has previously been observed (Weatherly, 2017; Weatherly *et al.*, 2018). Thus, to measure TCS effects on PMP, genetically encoded voltage indicators (GEVIs), which contain β-barrel protein structures which may protect their fluorophores from chemical quenching or aggregation effects (Chalfie and Kain, 2005), were used. Triclosan does not interfere with the fluorescence of the fluorescent protein within the reporter construct GCaMP (Weatherly *et al.*, 2018).

To measure PMP of cells using a GEVI, RBL cells were transiently transfected with ArcLight-A242 (ArcLight) (Jin *et al.*, 2012) (Figure 3.3A). The next day, confocal images were collected for each cell at different time points, up to 15 minutes, before (Figure 3.3A) and after (Figure 3.3B) addition of control (BT), TCS, or gramicidin. Fluorescence obtained was quantified using FIJI image J (Manual Image Analysis methods in Chapter 2) and normalized to the 0 min time point for each condition. Gramicidin, a known PMP depolarizer, statistically significantly reduces ArcLight fluorescence within 2 min of exposure and by 23% (± 2% SEM)

at the end of 7 minutes. TCS, at 20 µM, statistically significantly lowers ArcLight fluorescence within 5 min of exposure and by 25% (± 3% SEM) at the end of 15 min. This result was further confirmed by an automated image analysis method (Appendix Figure A.3). The 10 µM TCS data suggest an inhibition of ArcLight fluorescence by 15 min but were not statistically significant. The decrease in ArcLight fluorescence suggests that both gramicidin and TCS inhibit mast cell PMP.

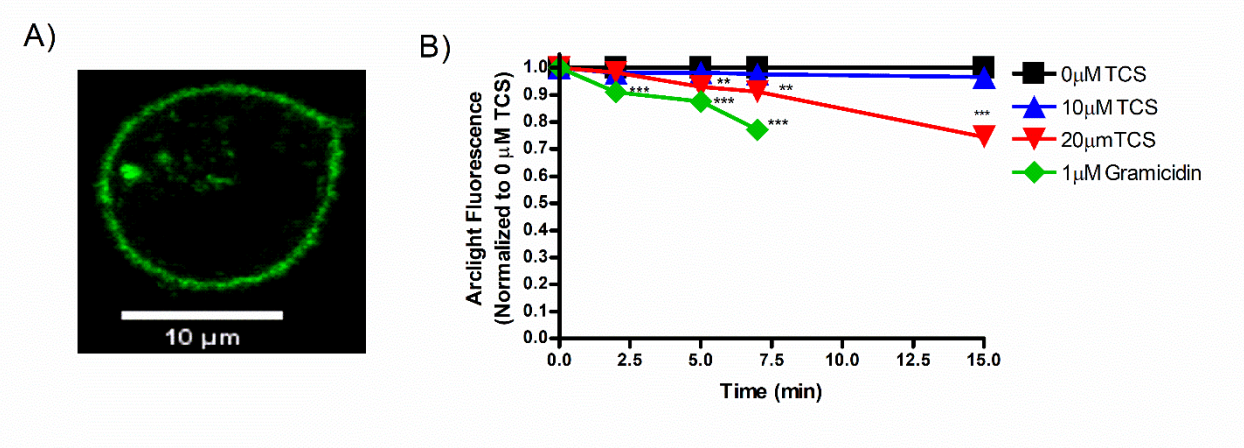

Figure 3.3. Triclosan and gramicidin effects on fluorescence of ArcLight-A242 in RBL mast cells. (**A**) One representative live-cell confocal microscopy image of an RBL mast cell transiently transfected with ArcLight construct, prior to gramicidin or TCS treatment. Scale bar, 10 µm**.** (**B**) RBL cells were transiently transfected with ArcLight, washed with BT, exposed to control (BT) (N = 52), 10 µM TCS (N = 22), 20 µM TCS (N = 28), or 1 µM gramicidin (N = 24) for 15 minutes. At each time point, the average fluorescence of each plasma membrane was measured, background-subtracted, and normalized to the 0 min timepoint, as described in Chapter 2. Values presented are means ± SEM of at least 3 independent days of experiments per treatment. Statistically significant results, as compared to the appropriate control (0µM TCS or 0µM gramicidin + DMSO vehicle), are represented by **p < 0.01, ***p < 0.001, as determined by one-way ANOVA followed by Tukey's post-hoc test.

Since gramicidin treatment contained DMSO vehicle (0.003%), it was important to determine whether gramicidin's effects on ArcLight fluorescence are modulated by the presence of DMSO. Thus, a control experiment was performed by repeating the gramicidin-ArcLight

experiments in the presence of varying DMSO concentrations. Gramicidin's ability to inhibit ArcLight fluorescence is unaffected by increasing DMSO concentrations, ranging from 0.003% to 0.02% (Appendix Figure B.1, B.2).

After experiments with transiently-transfected cells were successfully conducted, ArcLight stably-transfected cell lines were created, with the goal of enabling high-throughput testing of numerous concentrations of triclosan and other toxicants, as well as additional time points. However, unfortunately, clones of RBL cells stably transfected with ArcLight display construct aggregation and poor plasma membrane localization (Appendix Figure A.4).

To check whether plasmid expression level affects the change in GEVI fluorescence in response to triclosan, the initial, 0 min (pre-triclosan-exposure), background-subtracted mean fluorescence intensity of each individual cell from Figure 3.3's data was analyzed. The percentage drop in ArcLight fluorescence by 15 minutes time of exposure (control buffer-treated in 3.4A, TCS-treated in 3.4B), for each individual cell, was plotted as a function of that particular cell's initial mean intensity of ArcLight. There is no correlation between plasmid expression level and the magnitude of TCS inhibition of ArcLight fluorescence (Figure 3.4B), as analyzed by linear regression. Thus, TCS effects on GEVI fluorescence are unaffected by the "brightness" (GEVI expression level) of the cell.

In a random sample of 7 cells treated with 20 μM TCS, fluorescence distribution around the plasma membrane was obtained using the plot profile feature in Image J. Fluorescence values were obtained every 0.159 micron (=1 pixel) around the plasma membrane for individual cells, at 0 and 15 min post TCS treatment. Cells at 0 minute time point display a ~30% standard deviation in fluorescence pixels around each individual cell, similar to this distribution in cells that were exposed to triclosan for 15 minutes. This variation in fluorescence around the cell may be due to

differential delivery of constructs to different parts of the plasma membrane, differences in cell morphology at the chosen confocal slice imaged, or another reason. This ~30% average random error in Arclight fluorescence at various positions within the plasma membrane did not vary due to the presence or absence of triclosan. In contrast, in Figure 4, the triclosan data (4B) shows greater spread among individual cells than does the control data (4A), strongly suggesting that the spread in data due to triclosan is truly due to variable cellular responses to triclosan rather than due to and not due to pixel-by-pixel random error in fluorescence. Despite their clonality, individual RBL-2H3 mast cells are well known to respond variably to external stimuli (Millard *et al.*, 1988). Additionally, when standard deviation as a percentage of fluorescence values is plotted against distance around the plasma membrane, a fairly random distribution is seen in both groups of 0 and 15 minute TCS treated cells (data not shown). Together, these analyses bolster the conclusion that depression of Arclight fluorescence due to TCS exposure is a true cellular effect that is greater than random error.

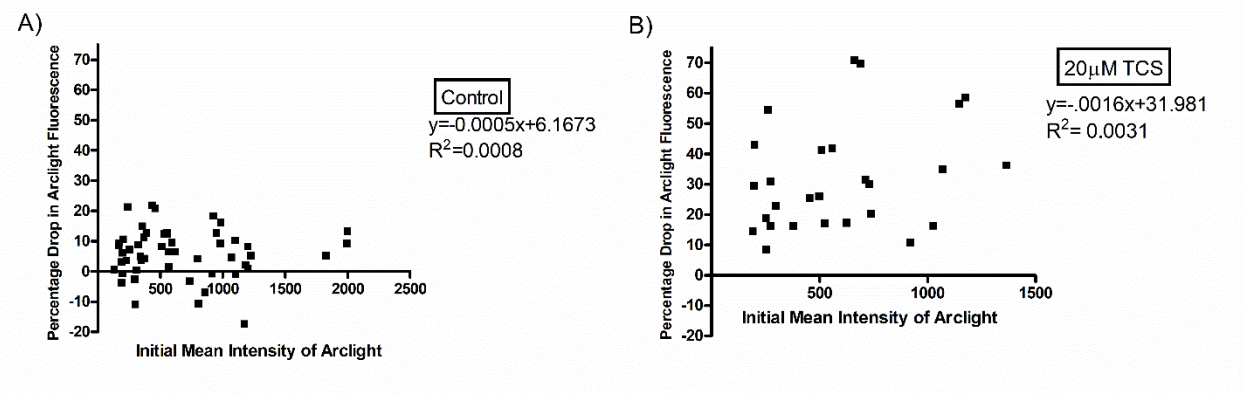

Figure 3.4. Effect of cellular expression level of ArcLight-A242 on TCS inhibition of ArcLight-A242 fluorescence. Data from Figure 3.3B, ArcLight-A242 transfected cells analyzed by confocal imaging and image analysis comparing control (0µM TCS) and 20µM TCS treatments, were plotted as individual cells' data. The percentage drop in fluorescence by 15

minutes time of exposure, for each individual cell, is plotted as a function of that cell's initial mean intensity of ArcLight-A242. Statistical results per plot are represented by equation of linear regression and R^2 values.

Plasma membrane depolarization causes ArcLight fluorescence intensity to decrease, in a linearly proportional fashion (Jin *et al.*, 2012). PMP percentage decline can be calculated from the measured change in ArcLight fluorescence, as outlined in Chapter 2. This apparent mast cell PMP, as a percentage of initial, 0 min, pre-triclosan-exposure value, is plotted as a function of time following TCS or gramicidin exposure (Figure 3.5). Within 7 min of exposure to 1 µM gramicidin, RBL mast cell PMP appears to decrease by 79% (± 7% SEM) of initial resting PMP, in a time-responsive manner. Similarly, within 15 min of exposure to 20 µM TCS, RBL cell PMP appears to decrease by 90% (± 11% SEM). There appears to be a modest, but not statistically significant, decline in PMP within 15 min exposure to 10 µM TCS.

Triclosan inhibits ArcLight fluorescence, and, thus, apparently inhibits RBL cell PMP. Thus, the next experiments tested whether these results are extendable to another immune cell type which is also dependent on PMP and SOCE for its function, T-cells.

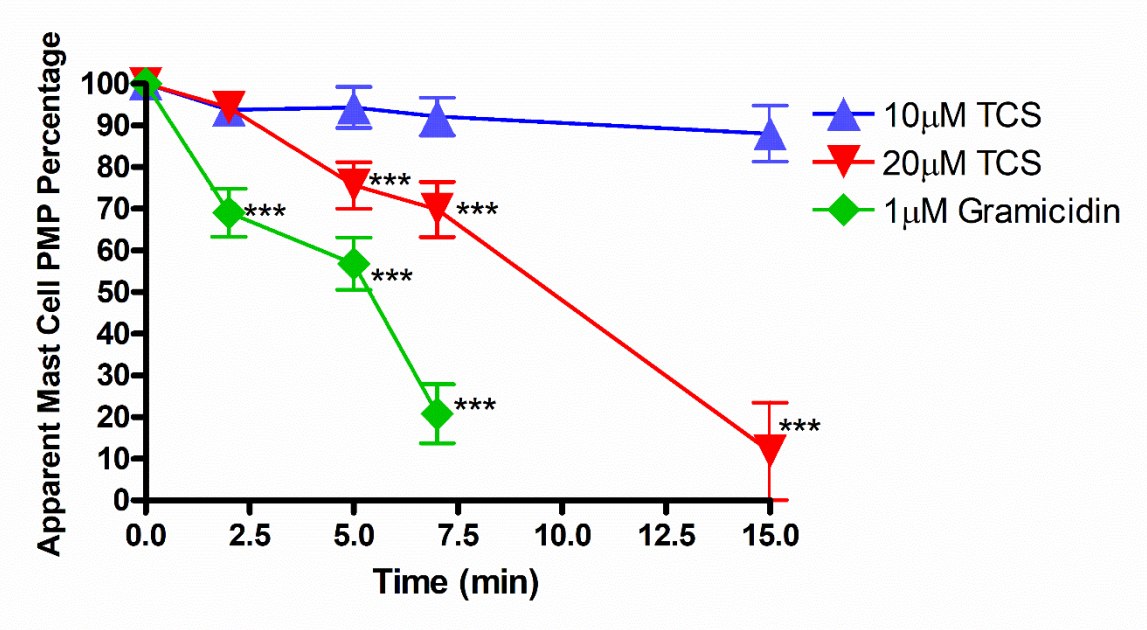

Figure 3.5. Triclosan and gramicidin apparent effects on plasma membrane potential (PMP) of RBL mast cells. Data from Figure 3.3B were utilized to calculate percentage of PMP (with each 0 min timepoint defined as 100%) as a function of time (min), as described in Chapter 2. Values presented are means ± SEM of at least 3 independent days of experiments per treatment. Statistically significant results, as compared to the appropriate control (0 μM TCS or 0 μM gramicidin + DMSO vehicle), are represented by ***$p < 0.001$, as determined by one-way ANOVA followed by Tukey's post-hoc test.

3.4 Non-cytotoxic doses of triclosan depress ArcLight-A242 fluorescence in Jurkat T cells.

To measure triclosan effects on PMP of T cells, human Jurkat T cells were transiently transfected with ArcLight. The next day, confocal images were collected for each cell at different time points, up to 15 minutes, before and after addition of control (BT) or TCS (Figure 3.6A). Fluorescence obtained was quantified using FIJI image J (Manual Image Analysis methods in Chapter 2) and normalized to the 0 min time point for each condition. TCS, at 20 μM, lowers ArcLight fluorescence within 2 min of exposure and by 31% (± 3% SEM) at the end of 15 min (Figure 3.6A). The decrease in ArcLight fluorescence suggests that TCS inhibits T cell PMP.

This apparent T cell PMP was calculated (see Chapter 2) as a percentage of initial, 0 min, pre-triclosan-exposure value and is plotted as a function of time following TCS exposure (Figure 3.6B). Within 15 min of exposure to 20 μM TCS, T cell PMP appears to decrease to -150% (± 15% SEM) of initial resting PMP, apparently a more-than-complete dampening of T cell PMP.

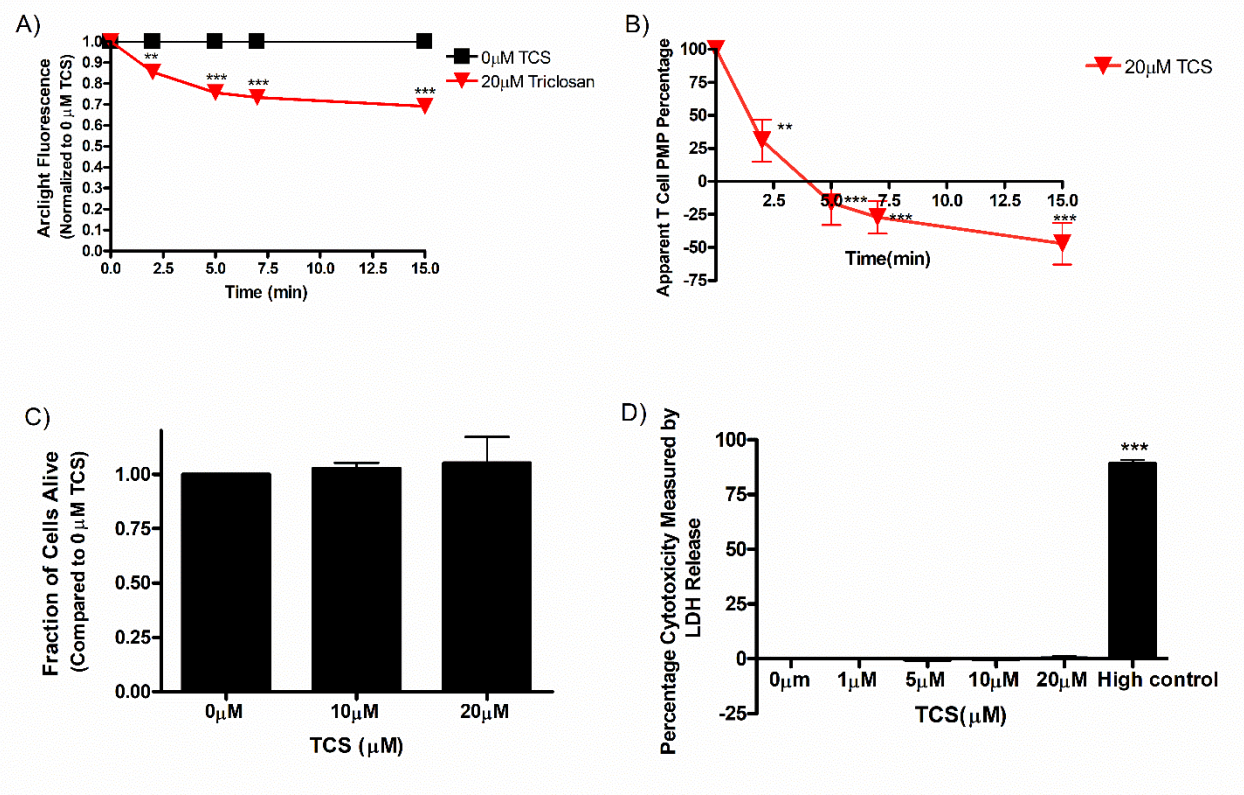

Figure 3.6. Triclosan effects on fluorescence of ArcLight-A242 in human Jurkat T cells, triclosan apparent effects on Jurkat plasma membrane potential (PMP), and cytotoxicity determination. **(A)** Jurkat cells were transiently transfected with ArcLight-A242, washed with BT, exposed to BT (0 μM TCS) (N=20) or 20 μM TCS (N=17) for 15 minutes. At each time point, the average fluorescence of each plasma membrane was measured, background-subtracted, and normalized to the 0 min timepoint, as described in Chapter 2. **(B)** Data from Figure 3.6A were utilized to calculate percentage of PMP (with each 0 min timepoint defined as 100%) as a function of time (min), as described in Chapter 2. **(C)** Jurkat T cell cytotoxicity to TCS was assessed by trypan-blue exclusion assay and by **(D)** lactate dehydrogenase (LDH) detection kit from Roche. "High control" is a sample treated with lysis solution provided by the kit. Values presented are mean ± SEM of at least three independent experiments. Statistically significant results, as compared to appropriate control, are represented by **p<0.01, ***$p < 0.001$, as determined by one-way ANOVA followed by Tukey's *post-hoc* test.

In order to determine if the results obtained above were truly functional changes or due to cytotoxicity from TCS, the effect of micromolar doses of TCS (0 μM, 10 μM, and 20 μM) on Jurkat T cell viability were assessed using a trypan blue exclusion assay. Results indicate that TCS does not cause a decrease in cell viability within a 30 min exposure (Figure 3.6C). In order to confirm these cytotoxicity results, a more sensitive microplate reader-based assay, LDH assay

was also performed. LDH release was measured in response to varying doses of TCS for 1 hour. There is no significant release of LDH from TCS-treated cells as compared to control; the "high control" sample is a positive control detecting LDH release from lysed cells (Figure 3.6D). These data from cytotoxicity experiments indicate that TCS dosage timing and concentration used in this study do not cause Jurkat T cell cytotoxicity.

3.5 Triclosan does not depress the fluorescence of the genetically encoded voltage indicator ASAP2 in RBL-2H3 mast cells.

To check the results obtained using ArcLight, an alternative GEVI, called ASAP2, which utilizes a different voltage-sensing mechanism from that of ArcLight (Jin *et al.*, 2012; Chamberland *et al.*, 2017) was used. RBL mast cells were transiently transfected with ASAP2 (Figure 3.7A). The next day, confocal images were collected for each cell at different time points, up to 15 minutes, before (Figure 3.7A) and after (Figure 3.7B) addition of control (BT) or TCS. Fluorescence obtained was quantified using FIJI image J (Manual Image Analysis methods in Chapter 2) and normalized to 0 min time point for each condition. Triclosan (20 μM, up to 15 min) does not alter fluorescence of ASAP2 when compared to the 0 μM TCS control (Figure 3.7B). In stark contrast to the clear triclosan dampening of fluorescence observed with the ArcLight reporter (Figure 3.3), these ASAP2 results (Figure 3.7B) indicate that TCS does not change the PMP of RBL mast cells.

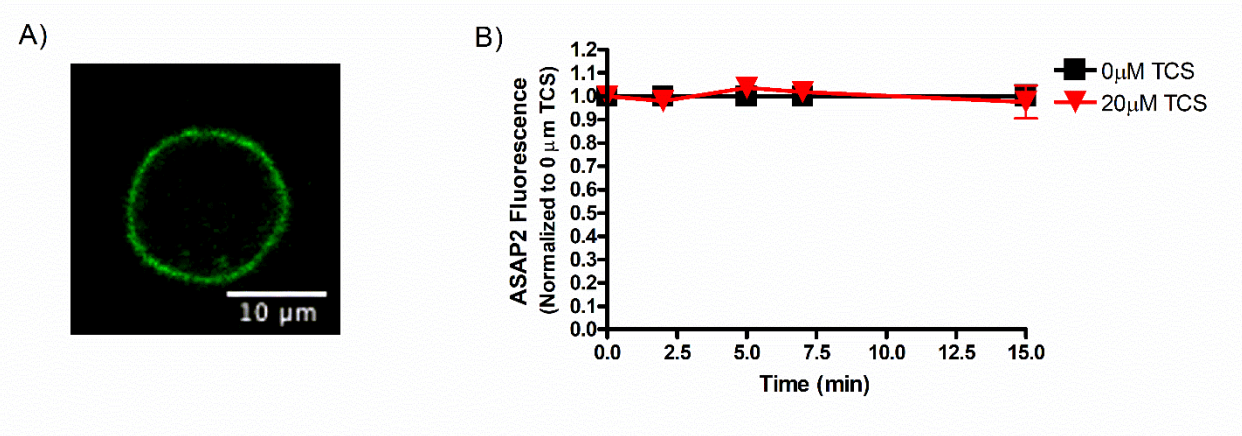

Figure 3.7. Triclosan effects on fluorescence of ASAP2 in RBL mast cells. (A) One representative live-cell confocal microscopy image of an RBL mast cell transiently transfected with ASAP2 construct, prior to TCS treatment. Scale bar, 10 µm**.** (**B**) RBL cells were transiently transfected with ASAP2, washed with BT, exposed to control (BT) (N=18) or 20 µM TCS (N=21) for 15 minutes. At each time point, the average fluorescence of each plasma membrane was measured, background-subtracted, and normalized to the 0 min timepoint, as described in Chapter 2. Values presented are means ± SEM of at least 6 independent experiments per treatment. Analysis by one-way ANOVA followed by Tukey's post-hoc test found no statistical significance.

However, TCS inhibits the fluorescence of ArcLight, which contains a pH-sensitive super ecliptic pHlourin on the cytoplasmic side of the plasma membrane. Thus, the next investigation centered on whether TCS-induced depression of ArcLight fluorescence is due to a change in cytosolic pH instead of a change in PMP.

3.6 Triclosan depresses fluorescence of a plasma membrane-targeted pHlourin in RBL mast cells, indicating triclosan reduction of cytosolic pH.

To identify whether TCS affects cytosolic pH, plasma membrane-targeted fluorescence reporter called Lyn-tailed mCherry-SEpHlourin (Koivusalo *et al.*, 2010), which measures sub-plasma membrane cytosolic pH of a cell, was employed. The transfection and imaging procedures used for the GEVI experiments were repeated, along with an automated image

analysis technique (described in Chapter 2). Triclosan, at 20 µM, decreases mCherry-SEpHlourin fluorescence intensity within 5 min of exposure and by 43% (± 2% SEM) at the end of 15 min (Figure 3.8). This result is similar to the magnitude of triclosan's effect on ArcLight fluorescence (Figure 3.3), suggestive of a pH change in response to TCS rather than a PMP change.

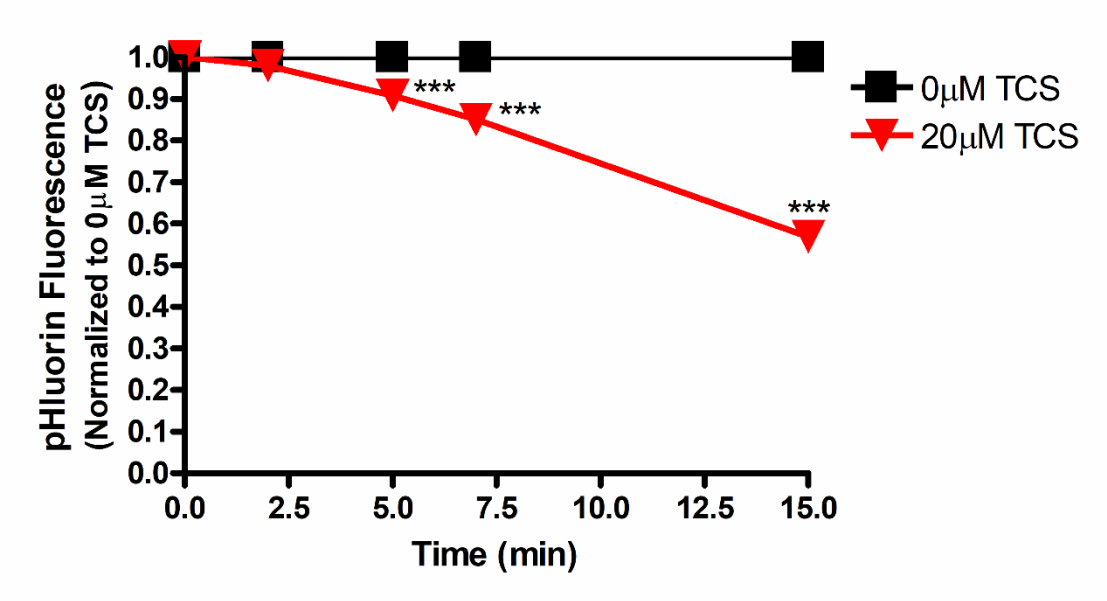

Figure 3.8. Triclosan effects on fluorescence of Lyn-tailed mCherry-SuperEcliptic (SE) pHluorin in RBL mast cells. RBL cells were transiently transfected with Lyn-tailed mCherry-SE pHluorin, washed with BT, and exposed to BT (N=35) or 20 µM TCS (N=52) for 15 minutes. At each time point, the average fluorescence of each plasma membrane was measured, background-subtracted, and normalized to the 0 min timepoint, as described in Image J Automated methods in Chapter 2. Values presented are means ± SEM of 3 independent days of experiments per treatment. Statistically significant results, as compared to the appropriate control (0µM TCS), are represented by ***$p < 0.001$, as determined by one-way ANOVA followed by Tukey's post-hoc test.

3.7 TCS inhibits cytosolic Ca^{2+} response to Anti-T Cell Receptor stimulation in Jurkat T cells

TCS affects Ca^{2+} dynamics and inhibits SOCE in mast cells (Weatherly *et al.*, 2018). Due to the similar triclosan depression of ArcLight fluorescence in Jurkat T cells (Figure 3.6A) as in RBL mast cells (Figure 3.3B), we hypothesized that a similar calcium effect also occurs in Jurkat T cells. To test this hypothesis, Jurkat T cells were transfected with Ca^{2+} reporter construct GCaMP6 (Chen *et al.*, 2013). The next day, cells were stimulated with 0.2 µg/ml Anti-T Cell Receptor (TCR) OKT3 ± TCS (Holowka *et al.*, 2018), and cytosolic Ca^{2+} was measured throughout the duration of 1 hour. Cells were transfected at a highly efficient rate (Appendix Figure A.5). Following anti-TCR stimulation, an initial rise in Ca^{2+} is seen within the first few minutes, followed by a plateau Ca^{2+} level above unstimulated basal level (compare "0 µM TCS + Ab" to "Unstimulated" curves in Figure 3.9A), as expected (Holowka *et al.*, 2018). TCS, at 20 µM, inhibits Ca^{2+} levels in comparison to the control in anti-TCR activated cells, in particular by flattening the plateau region (Figure 3.9A). Triclosan minimally affects the initial Ca^{2+} rise but heavily dampens calcium in the plateau region, similar to its effects in RBL mast cells (Weatherly *et al.*, 2018). AUC analysis reveals an average decrease of 70% (± 17%) integrated Ca^{2+} levels in anti-TCR activated cells with TCS treatment compared to that of activated control (Figure 3.9B). These data indicate that TCS inhibits cytosolic Ca^{2+} signaling in T cells.

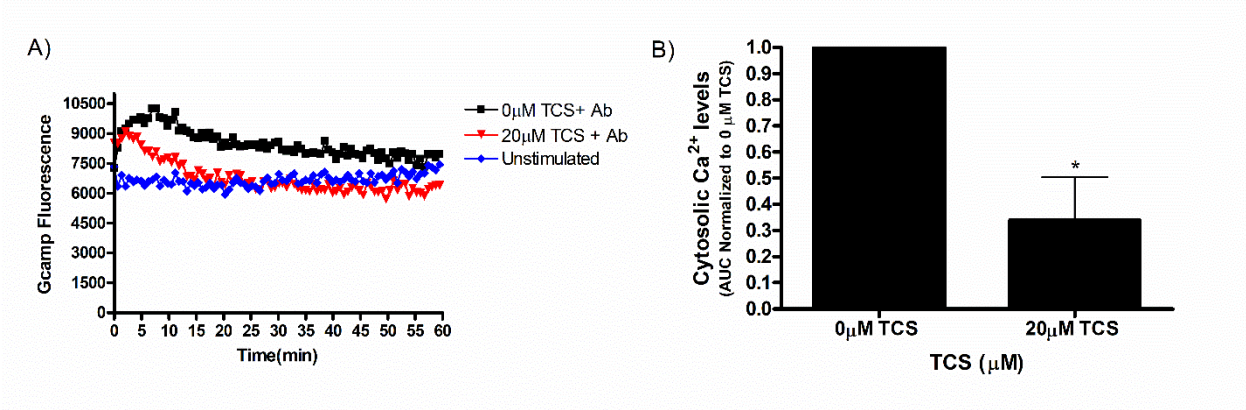

Figure 3.9. **Triclosan effects on cytosolic Ca^{2+} levels as activated by anti-T Cell Receptor (TCR) antibody in Jurkat T Cells**. Jurkat cells were transiently transfected with cytosolic GCaMP6 overnight, then exposed in BT Control or 20 μM TCS, each with 0.2 μg/ml anti-TCR ("Ab") for 1 hour. "Unstimulated" contained no TCS and no anti-TCR. Raw fluorescence was measured using a microplate reader as described in Chapter 2. **(A)** Representative figure (no error bars) shows fluorescence obtained following background fluorescence subtraction (mock-transfected cells' fluorescence) from treatment groups at each time point. **(B)** Area under the curve (AUC) was obtained from the fluorescence curves and values were normalized to the control of each day for 3 replicates per treatment group per day. AUC values presented are means ± SEM of 3 independent days of experiments. Statistically significant results, as compared to the appropriate control (0μM TCS), are represented by *$p < 0.05$, as determined by unpaired t-test.

CHAPTER 4

DISCUSSION

Triclosan disrupts mast cell function, rapidly (within tens of minutes) and at non-cytotoxic concentrations relevant to consumer product exposure (Palmer *et al.*, 2012; Shim *et al.*, 2019), but the underlying biochemical mechanism was unknown. In this study, we unraveled the mode of action of TCS in mast cells and replicated these TCS effects in another immune cell type, T cells.

The process of deciphering the mechanism began with two observations: TCS is a mitochondrial uncoupler (Weatherly *et al.*, 2016; Weatherly *et al.*, 2018) and also a disruptor of the central signal for mast cell degranulation—cytosolic Ca^{2+} rise (Weatherly *et al.*, 2018). As an uncoupler, TCS depresses the MMP, which results in mitochondrial fragmentation, observed in live cells with super-resolution microscopy (Weatherly *et al.*, 2018). Mitochondrial toxicity and deformation are important markers of TCS toxicity in numerous cell types and species (Shim *et al.*, 2016; Weatherly *et al.*, 2018; Weatherly *et al.*, 2020). Disruption of mitochondrial shape plays a role in diseases such as cognitive decline (Hara *et al.*, 2014), Parkinson's disease (Cui *et al.*, 2010; Bhandari *et al.*, 2014), insulin resistance (Jheng *et al.*, 2012), immune dysfunction (Weatherly *et al.*, 2020), inflammation (Compan *et al.*, 2012), and disrupted embryonic development (Chen *et al.*, 2003). In this study (Figure 3.1), we have augmented these findings by utilizing 3D super-resolution FPALM to reveal TCS enhancement of mitochondrial surface area and volume, indications of mitochondrial swelling and MMP disruption (Guillery *et al.*, 2008; Giedt *et al.*, 2012). This increase in surface area and volume has also been observed in neuronal mitochondria due to exposure to carbonyl cyanide-4 (trifluoromethoxy)phenylhydrazone (FCCP), a known proton ionophore and MMP depolarizer (Safiulina *et al.*, 2006). The connections between mitochondrial deformation and disrupted MMP

are extended to PMP depolarization, inhibited store-operated calcium entry (SOCE), and, subsequently, dampened mast cell degranulation via studies with a similar proton ionophore mitochondrial uncoupler, carbonyl cyanide *m*-chlorophenylhydrazone (CCCP), which also inhibits MMP, PMP, SOCE, and mast cell degranulation (Mohr and Fewtrell, 1987b). Triclosan's enhancement of mitochondrial surface area and volume led to a PMP collapse hypothesis as the mode of action of immune cell dysfunction.

Data from figure 3.1 were replotted to obtain a relationship between surface area and volume of mitochondria of control and 20 μM TCS treated cells. Figure 4.1 shows variation in cell responses to control and TCS, showing that when mitochondria in cells increase in surface area due to TCS, they also increase in volume linearly. However, due to complexity of mitochondria and their networks, we cannot conclude if this uniform change is reflected in mitochondria shape.

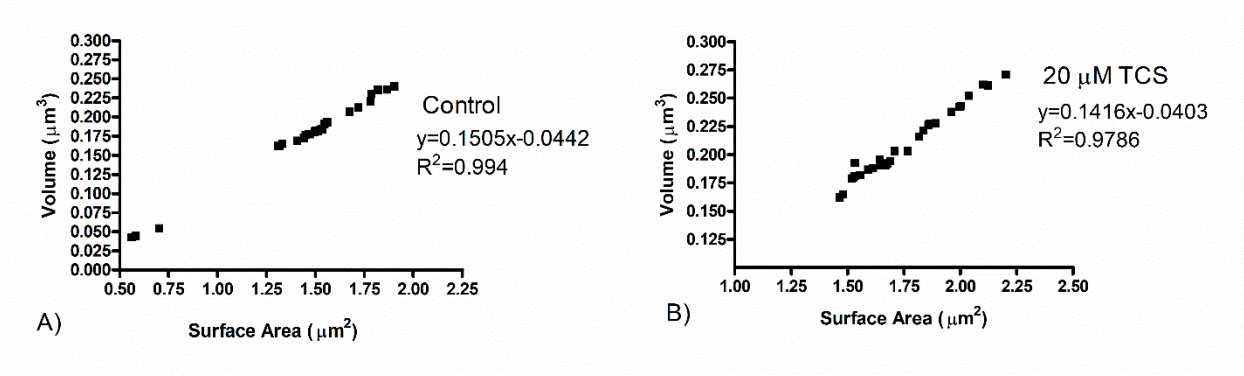

Fig 4.1. Relationship between mitochondrial surface area and volume. Data from figure 3.1 were replotted to get a relationship between mitochondrial surface area and volume from control (A) and 20 μM TCS (B) treated cells. Statistical results in the plot are represented by equation of linear regression and R^2 values.

Thus, we hypothesized that TCS inhibits not just MMP but also PMP. Direct evidence for this hypothesis was provided by reports that TCS induces a current (evidence of its proton ionophore nature) across artificial membranes (Popova *et al.*, 2018) and depolarizes neuronal PMP (Arias-Cavieres *et al.*, 2018; Popova *et al.*, 2018) at micromolar doses within tens of minutes. As calculated in the Introduction, a complete depolarization of PMP in mast cells would lead to a ~45% reduction in the driving force for cytosolic Ca^{2+} influx into the cell through activated CRAC channels; indeed, Weatherly et al., 2018 reported ~45% decrease in cytosolic calcium levels after TCS exposure in RBL mast cells. This study also reports (Figure 3.9) a robust decrease in cytosolic calcium levels after TCS exposure in Jurkat T cells. In turn, the decrease in cytosolic Ca^{2+} inhibits degranulation (Holowka *et al.*, 2012). Additionally, the known PMP depolarizer gramicidin inhibits mast cell degranulation in parallel conditions to TCS mast cell disruption (Figure 3.2), lending further support for the PMP collapse hypothesis for the TCS mode of action.

To measure TCS effects on PMP, two genetically encoded voltage indicator (GEVI) reporter constructs, ArcLight-A242 (ArcLight) (Jin *et al.*, 2012) and ASAP2 (Chamberland *et al.*, 2017), were utilized. ArcLight senses changes in PMP due to its two specialized subunits: a transmembrane voltage-sensing domain which, upon changes in PMP, undergoes conformational changes that cause conformational changes in the attached green fluorescent protein (GFP)-derived, super ecliptic pHlourin fluorescent domain which is localized intracellularly, in the cytosol. ASAP2 also contains a transmembrane voltage-sensing domain but, in contrast to ArcLight, ASAP2 contains an extracellularly-located, circularly-permuted (non-pHlourin-based) fluorescent GFP (cpGFP) domain. For both of these GEVIs, their fluorescence intensity decreases upon PMP depolarization. These experiments yielded drastically different results:

Triclosan inhibits ArcLight fluorescence in RBL mast cells (Figure 3.3) and in Jurkat T cells (Figure 3.6), suggesting TCS-induced collapse of PMP in these cell types (Figures 3.5 and 3.6). Note that the effect was not statistically significant with 10 μM TCS but did suggest a modest inhibition at that dose/timeframe. In contrast, TCS had no effect on ASAP2 fluorescence (Figure 3.7). While both ArcLight and ASAP2 are plasma membrane voltage-sensitive, there is a crucial difference in their structures: the location and pH sensitivity of their fluorescent protein domains. ArcLight's fluorescent domain is a pHlourin, which is strongly pH-sensitive in the physiological pH range (Jin *et al.*, 2012) (Supplemental Figure 2B from this article shows that a pH reduction from 7.5 to 6.5 would drastically reduce this pHlourin's intensity, by ~50% or more). It is located in the cytosol, so it reports changes in cytosolic pH, with acidification leading to fluorescence intensity decline. ASAP2 cannot report cytosolic pH changes because its fluorescent domain is located outside the cell, unless those changes affect the PMP (personal communication, Dr. Francois St-Pierre). Interpretation of the ASAP2 data is somewhat confounded by the fact that its cpGFP fluorescent domain is also somewhat pH sensitive (Miyawaki and Niino, 2015; Kostyuk *et al.*, 2019). It is possible that TCS could cause extracellular acidification, which would affect ASAP2 fluorescence, as a consequence of its mitochondrial toxicity, but a previous report of extracellular acidification due to TCS exposure was shown after 44 hours of exposure (Ajao *et al.*, 2015) while our GEVI experiments were completed in 15 min. Also, if TCS were acidifying the extracellular space around the RBL mast cells and Jurkat T cells within the experimental exposure time (15 min), overcoming the buffering of the BT solution, a decrease in ASAP2 fluorescence would have occurred (Stepanenko *et al.*, 2008). Together, these data suggest that TCS does not affect mast cell or T cell PMP but, instead TCS lowers cytosolic pH.

Indeed, TCS acidifies the cytosol, as measured with lyn-tailed mCherry-SEpHluorin, a pH-sensitive, PMP-insensitive reporter construct (Figure 3.8). ArcLight and lyn-tailed mCherry-SEpHluorin share the same pH-sensitive fluorophore, the super ecliptic pHlourin (Koivusalo *et al.*, 2010; Jin *et al.*, 2012). A decrease in lyn-tailed mCherry-SEpHluorin's fluorescence is equivalent to a cytosolic pH decrease (Koivusalo *et al.*, 2010). This intracellular pH effect may either be localized, or be most drastic, near the plasma membrane itself as both of these pH-sensitive reporters are plasma membrane-localized (Koivusalo *et al.*, 2010; Jin *et al.*, 2012). As noted in Chapter 2, a 35% decrease in the fluorescence intensity of ArcLight corresponds with a 100 mV PMP decrease (Jin *et al.*, 2012); thus, a 29% decrease in fluorescence intensity would correspond with a complete depolarization of the RBL cell PMP (~82.5mV) (Lindau and Fernandez, 1986; Wischmeyer *et al.*, 1995). Thus, if the ArcLight response were measuring PMP changes in response to TCS, the maximum response of any cell should have been ~29%. On the contrary, nearly half of cells responded to TCS exposure with a greater-than-29% drop in ArcLight fluorescence (Figure 3.4). Some of this variation is likely due to cell-to-cell variation in signaling, even in this clonal cell line (Millard *et al.*, 1988).

However, because ArcLight's fluorescence can also communicate changes in pH and can be depressed nearly 100% within a 1 pH unit acidification starting at normal physiological pH (Jin *et al.*, 2012), the cell-to-cell variation of TCS response in Figure 3.4 provides further evidence for TCS acidification of the cytosol.

Taking into account the pH sensitivity of its fluorophore (Jin *et al.*, 2012), the ArcLight data (Figure 3.3) can be re-interpreted as a 20 μM TCS-induced pH decrease of -0.23 pH units (Table 4.1). The pH sensitivity of the fluorescence intensity of ArcLight's super ecliptic A227D pHlourin (plotted in the Supplement of (Jin *et al.*, 2012)) is approximately linear between pH 6.5

to 7.5. This relationship can be approximated using the following: $F = 0.6pH - 3.8$ where F is the fraction of maximal fluorescence, and the equation is valid over a range of ± 0.5 pH units. Thus, at a pH of 7.2, F = 0.52, meaning that ArcLight will exhibit 52% of its maximal fluorescence intensity at the starting, physiological pH. The 26% ± 3% (SEM) decline in ArcLight fluorescence due to 15 min of 20 μM TCS exposure (Figure 3.3) translates to a 26% reduction in this 0.52 value, bringing the final, normalized, ArcLight fluorescence intensity to 0.38 ± 0.02; solving for the corresponding pH value returns a final pH value of 6.97 ± 0.02 following this TCS exposure. This yields the -0.23 pH unit decrease estimate from the ArcLight data (Table 4.1). Additionally, the same data interpretation can be employed with lyn-tailed mCherry-SEpHluorin, resulting in a pH decrease to 6.83 ± 0.02, yielding the -0.37 pH unit decrease estimate (Table 4.1). These pHlourin-measured decreases in pH are similar in magnitude, providing corroborating evidence that TCS acidifies the cytosol.

Method	**Magnitude of pH Change**	**Citation**
Calculated estimate	-0.3	Discussion
ArcLight experiments	-0.23	**Figure 3.3**
pHlourin experiments	-0.37	**Figure 3.8**
Average	-0.3	**Table 4.1**

Table 4.1. Summary of estimated changes in cytosolic pH following TCS exposure.

These measured pH changes were confirmed with theoretical calculations of TCS acid-base chemistry. Taking into account the 400 µL volume of 20 µM TCS in each ibidi well containing ~400,000 cells on each experimental day (see Chapter 2), along with an estimated 10% absorption rate (Moss *et al.*, 2000; Weatherly and Gosse, 2017), each cell received ~5.3 x 10^{-15} moles, or 3.2 x 10^{9} molecules of TCS. Considering its pKa of 7.9 (PubChem), a resting cell cytosolic pH of 7.2 (Johnson *et al.*, 1980; Lodish *et al.*, 2000; Beck *et al.*, 2014), and the Henderson-Hasselbalch equation, 16.6% of TCS is deprotonated when it encounters the pH 7.2 resting cytosol. This 16.6% value equates to 5.3 x 10^{8} deprotonated TCS molecules per cell, and hence, 5.3 x 10^{8} excess H^{+} delivered to each cell as this monoprotic weak acid dissociates. While this excess proton dose, from TCS, far exceeds the proton concentration of the cell, it rapidly encounters the cellular buffering system. Carbonate (CO^{2}/HCO_{3}^{-}, pKa 6.1) buffering (Nelson and Cox, 2017) accounts for approximately two-thirds of a cell's total buffering power (Boron, 2004), and average mammalian cells contain 12 mM of HCO_{3}^{-} (Lodish *et al.*, 2000), the conjugate base of this buffering system (A^{-}); these values and the Henderson-Hasselbalch equation can be used to calculate the concentration of the weak acid (HA) in the untreated cell: 0.953 mM. The average mammalian cell has a volume of 1766 μm^{3} (Barrandon and Green, 1985), and the cytosol itself accounts for 70% cellular volume (Luby-Phelps, 2000). Thus, the volume of the cytosol is 1236 μm^{3} or 1.236 x 10^{-12} L. Multiplying this volume by the HA and A^{-} concentrations noted above and by Avogadro's number yields the number of HA and A^{-} molecules found within the cytosol of an untreated cell: 7.1 x 10^{8} HA molecules and 8.9 x 10^{9} A^{-} molecules. The 5.3 x 10^{8} excess H^{+} delivered to the cell by TCS exposure interact 1:1 with these A^{-} molecules, thereby producing 5.3 x 10^{8} new HA molecules added to the original pool of HA molecules and subtracted from the original pool of A^{-} molecules: resulting in 1.24 x 10^{9}

molecules of HA and 8.4 x 10^9 A^- molecules. Plugging these values into the Henderson-Hasselbalch equation leads to a cytosolic pH of TCS-treated cells of 6.9: a -0.3 pH depression caused by TCS exposure (Table 4.1). In fact, the average of the pH depressions captured in the ArcLight and lyn-tailed mCherry-SEpHluorin measurements is -0.3, in agreement with this calculated value.

Acidification of the cytosol has been shown to decrease Ca^{2+} release-activated Ca^{2+} current (I_{CRAC}), the final step in SOCE, in several cell types including RBL and Jurkat T cells expressing stromal interaction molecule 1 (STIM1) and ORAI1 (Beck *et al.*, 2014). In this study, the cytosol of each assayed cell was acidified via direct introduction of NaOH or HCl via pipette. A stepwise effect, reduction of I_{CRAC} occurred upon decreasing the pH from 7 to 6. Triclosan-mediated acidification of the cytosol may thus explain the previously observed inhibition of Ca^{2+} dynamics (Weatherly *et al.*, 2018) and, thus, of degranulation (Holowka *et al.*, 2012).

Another proton ionophore mitochondrial uncoupler, CCCP, also inhibits Ca^{2+} influx into RBL mast cells (Mohr and Fewtrell, 1987b). While this effect is partly caused by CCCP's depolarization of PMP (Mohr and Fewtrell, 1987b), it can also be reversed by increasing the pH (i.e. alkalization) of the surroundings (Mohr and Fewtrell, 1987b) and, hence, of the cytosol because H^+ becomes plasma membrane-permeant when CCCP is incorporated into the membrane (McLaughlin and Dilger, 1980). These findings suggest that CCCP inhibition of SOCE is partly caused by its pH modulation. Additionally, experiments on isolated neurons have shown that another proton ionophore mitochondrial uncoupler, FCCP, also acidifies the cytosol (Tretter *et al.*, 1998). Therefore, TCS is acting as expected, from its proton ionophore mitotoxicant nature, in acidifying the immune cell cytosol and, then, inhibiting SOCE.

While under some conditions acidification of the cytoplasm can inhibit SOCE by blocking the binding of IP_3 to its receptor on the ER (Tsukioka *et al.*, 1994), release of Ca^{2+} from the ER is actually enhanced in TCS-treated mast cells (Weatherly *et al.*, 2018). Following anti-TCR activation of SOCE in T cells, the initial rise of Ca^{2+} release from the ER is largely unaffected by TCS whereas the plateau region representing SOCE via CRAC channels is heavily reduced by TCS (Figure 3.9), further evidence that IP_3 receptor interference is not the key mechanism of TCS inhibition in T cells, as well. Instead, it is likely that TCS-induced cytosol acidification blocks the proper interaction of the STIM and ORAI1 machinery that is required for CRAC channel opening (Thompson *et al.*, 2009; Mancarella *et al.*, 2011). Histidine 155, found between transmembrane domain (TM) 2 and 3 of ORAI1, plays an important role in sensing intracellular pH (Tsujikawa *et al.*, 2015). Upon cytoplasmic acidification, H155 becomes protonated and affects intermolecular interaction of other components in the loop between TM2 and TM3 of the ORAI1 that may result in CRAC channel closing (Tsujikawa *et al.*, 2015). This histidine is conserved in rat (as in RBL cells) and human (as in the Jurkat T cells), according to an NCBI Blast multiple amino acid sequence alignment. TCS-induced protonation and closing of CRAC channels reduces influx of Ca^{2+} into mast cells (Weatherly *et al.*, 2018) and T cells (Figure 3.9) and inhibits mast cell function (Palmer *et al.*, 2012).

Future research will examine inhibition of T cell functions downstream of SOCE, such as release of essential cytokines (Punt *et al.*, 2019). In addition to the known TCS inhibition of mast cell degranulation and other functions (Palmer *et al.*, 2012), TCS also inhibits the lytic function of natural killer cells (Udoji *et al.*, 2010; Hurd-Brown *et al.*, 2013), which are important defenders against cancer and viral infections.

In addition to acidifying the cytosol by its direct proton ionophore mechanism of providing a pathway for charged protons to flow into the cell, TCS may also be acidifying the cell contents via other mechanisms. TCS increases the production of reactive oxygen species (ROS) in mast cells (Weatherly *et al.*, 2018) and in other cell types (Binelli *et al.*, 2009; Riva *et al.*, 2012; Tamura *et al.*, 2012; Yueh *et al.*, 2014; Lv *et al.*, 2016; Weatherly *et al.*, 2018), which impair the Na/H^+ exchanger, leading to reduced intracellular pH (Kaufman *et al.*, 1993; Nakamura *et al.*, 2006). TCS also causes mitochondrial fission/fragmentation (Weatherly *et al.*, 2018), processes associated with reduced intracellular pH as a result of lactic acid buildup attributed to increased glycolysis (Johnson and Nehrke, 2010; Schurr, 2014). While the timeframes in which these processes acidify the cell are likely longer than the rapid (within 15 min) acidification reported in this study, these mechanisms suggest that TCS will continue to acidify the cell over longer exposure times and possibly at lower doses; ROS stimulation and mitochondrial dysfunction occur in primary human keratinocytes, mast cells, and other cell types at lower doses (starting ~1 μM) than the 10-20 μM used in the current study.

If this TCS acidification occurs in the mitochondria to a similar degree (~0.3 pH unit acidification of the matrix), the driving force (Gibbs free energy) available for producing ATP on ATP synthase in the inner mitochondrial membrane will be also reduced, as previously observed (Weatherly *et al.*, 2016). This effect can be estimated by calculating the driving force both in the presence and absence of 20 μM TCS, via the equation

$$\Delta G_{Transport} = 2.3RT\Delta pH + \mathrm{F}\Delta\Psi$$

(Nelson and Cox, 2017). Using the 37°C temperature used experimentally, the gas and Faraday's constants, ΔpH = -0.75, and $\Delta\Psi$ = -0.2 V (Nelson and Cox, 2017), the free energy released by protons flowing through ATP synthase into the matrix is a robust ~-24 kJ/mol in a

healthy cell. Taking into account a 0.3 pH unit acidification of the matrix (such that ΔpH = -0.45) and a 40% reduction in $\Delta\Psi$ (Weatherly *et al.*, 2018) due to 20 μM TCS exposure, the free energy released by protons flowing through ATP synthase into the matrix is a weaker ~-14 kJ/mol in a TCS-treated cell. This result implies a ~40% reduction in the free energy available for making ATP. While imperfect, this value is a reasonable match to the >50% reduction in ATP production caused by 20 μM TCS in RBL cells (Weatherly *et al.*, 2016).

TCS inhibits MMP (Weatherly *et al.*, 2018); however, TCS does not inhibit PMP. This apparent contradiction can be explained by the inherent cellular mechanisms in charge of creating and then maintaining either the MMP or the PMP. The MMP is primarily generated by the action of the electron transport chain (ETC) proton pumps (Nelson and Cox, 2017); MMP is entirely reliant on this segregation of protons. TCS is a proton ionophore mitochondrial uncoupler, thus, acting in direct opposition to the proton pumps of the ETC (Weatherly *et al.*, 2016). Such direct opposition, with no alternative means of MMP maintenance, serves to explain why TCS can significantly depress the MMP. In contrast to the MMP's generation by proton pumping, PMP is primarily generated by the action of the Na^+/K^+ ATPase, (Nelson and Cox, 2017), which is located nearly exclusively on the plasma membrane (Bertorello *et al.*, 2003) and is not present on the mitochondrial membrane. In RBL mast cells, the Na^+/K^+ ATPase contributes to PMP (Bronner *et al.*, 1989) and resides on the plasma membrane of RBL cells, and its inhibition leads to dampening of Ag-stimulated degranulation (Gentile and Skoner, 1996). Thus, TCS modulation of proton concentrations could affect cytosolic pH without altering PMP. TCS does cause PMP depolarization of artificial membranes which do not contain the Na^+/K^+ ATPase (Popova *et al.*, 2018). TCS-mediated changes in proton concentrations across these membranes would therefore not be counteracted by the Na^+/K^+ ATPase. TCS also causes PMP

depolarization of neuronal models (Arias-Cavieres *et al.*, 2018; Popova *et al.*, 2018) at micromolar doses within tens of minutes. Neurons heavily rely on the PMP for their function and, while the Na^+/K^+ ATPase is still the primary source of this voltage, neurons possess additional PMP regulation mechanisms (Bean, 2007), which may explain triclosan's differential effects on PMP of immune cells vs. neuronal cells. Interestingly, TCS inhibits Na^+/K^+ ATPase activity in *Labeo rohita* gills (Hemalatha *et al.*, 2019), a hint that, over longer exposure periods than those used in the current study, TCS may interfere with cellular PMP. Na^+/K^+ ATPase uses ATP to function properly (Nelson and Cox, 2017). TCS (20μM) significantly inhibits ATP production in cells in galactose media, conditions under which they are forced to undergo oxidative phosphorylation (Weatherly *et al.*, 2016). Could TCS inhibit mast cell degranulation by inhibiting Na^+/K^+ ATPase function through reduced ATP production? When mast cells are placed in glucose media (BT), 20 μM TCS only inhibits ATP production by 8% (Weatherly *et al.*, 2016). This small inhibition of ATP does not explain the 80% reduction in degranulation, experiments which are performed in glucose-containing media, in response to 20μM TCS (Weatherly *et al.*, 2016; Weatherly *et al.*, 2018).

In conclusion, we report the mechanism of TCS inhibition of mast cells and T cells (Figure 4.1). Three-dimensional super-resolution microscopy shows that TCS causes mitochondrial swelling in mast cells, further evidence for its depolarization of the mitochondrial membrane. However, TCS does not inhibit immune cells by dampening their plasma membrane potential. Using genetically encoded voltage indicators coupled with pH-indicating reporters, we have identified that TCS acidifies the cytosol but does not affect PMP in immune cells. Cytosolic acidification disrupts the Stim1-Orai1 interaction, causing CRAC channel closing and collapse of Ca^{2+} influx into mast cells and T cells. TCS-induced reduction of Ag-stimulated cytosolic Ca^{2+}

influx results in inhibited enzymatic activity and decreased microtubule polymerization, leading to suppression of mast cell degranulation. Collapse of SOCE in T cells also likely leads to inhibition of T cell function. Any cell type that depends on Ca^{2+} signaling or mitochondrial function is susceptible to TCS toxicity (Feske, 2007; Hill-Eubanks *et al.*, 2011). In summary, TCS, a mitochondrial toxicant, is also an immunotoxicant via its modulation of immune cell signal transduction.

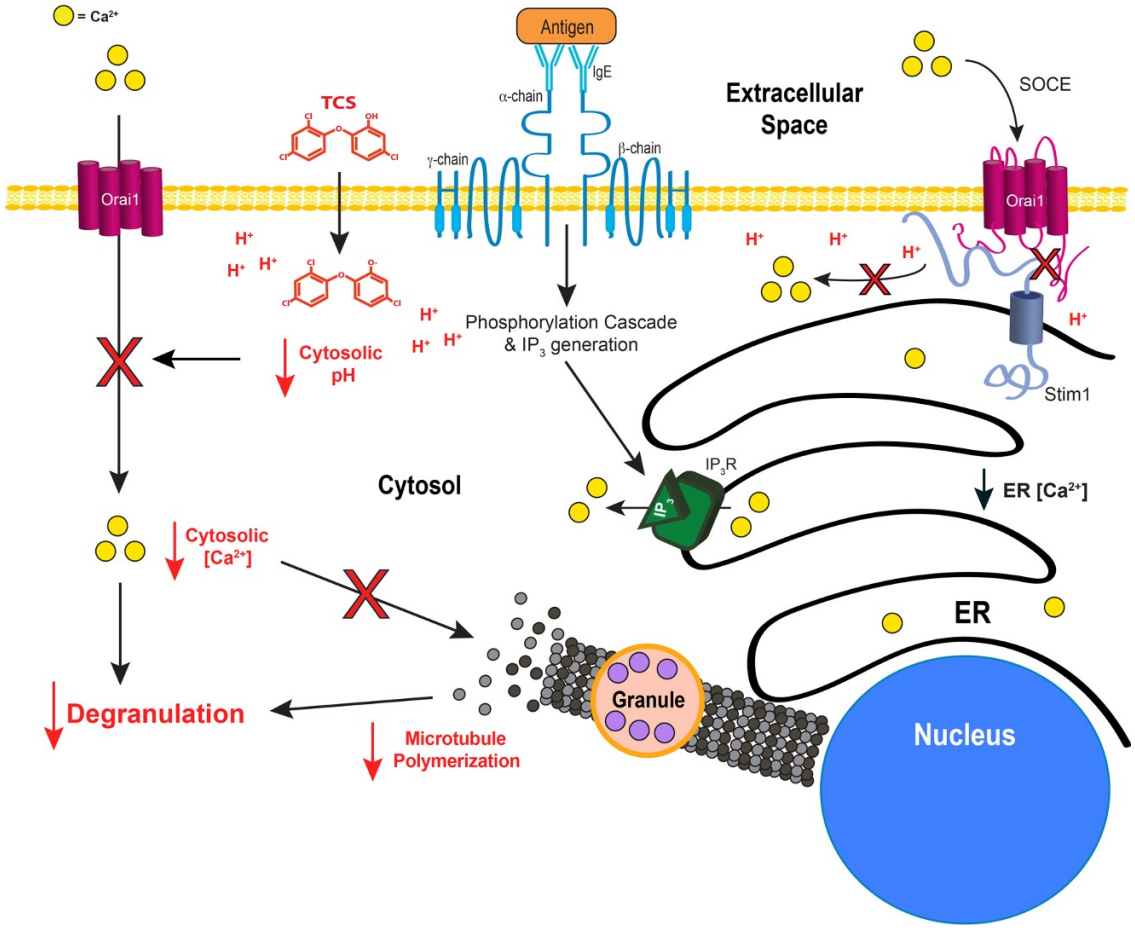

Figure 4.2. Schematic diagram of TCS effects on mast cell degranulation through CRAC channel inhibition. When multivalent Ag activates mast cells, they undergo series of phosphorylation cascades and form IP_3, which binds to the ER, resulting in a decrease in ER Ca^{2+}. This depletion of ER Ca^{2+} causes STIM1 to associate with ORAI1 and activate SOCE, resulting in an influx of Ca^{2+} into the cytosol through the CRAC channel. Using previous and current findings, we conclude that TCS-led cytosolic acidification disturbs the interaction

between STIM1 and ORAI1, resulting in a decreased influx of Ca^{2+} through the CRAC channel. Dampened cytosolic calcium inhibits microtubule polymerization and inhibits enzyme activation: combined together, these effects result in TCS inhibition of mast cell degranulation.

REFERENCES

Abramson, J., Pecht, I., 2007. Regulation of the mast cell response to the type 1 Fc epsilon receptor. Immunol Rev **217**, 231-254.10.1111/j.1600-065X.2007.00518.x

Ajao, C., Andersson, M.A., Teplova, V.V., Nagy, S., Gahmberg, C.G., Andersson, L.C., Hautaniemi, M., Kakasi, B., Roivainen, M., Salkinoja-Salonen, M., 2015. Mitochondrial toxicity of triclosan on mammalian cells. Toxicology reports **2**, 624-637.10.1016/j.toxrep.2015.03.012

Alsaleh, N.B., Persaud, I., Brown, J.M., 2016. Silver Nanoparticle-Directed Mast Cell Degranulation Is Mediated through Calcium and PI3K Signaling Independent of the High Affinity IgE Receptor. PloS one **11**, e0167366.10.1371/journal.pone.0167366

Anderson, S.E., Meade, B.J., Long, C.M., Lukomska, E., Marshall, N.B., 2016. Investigations of immunotoxicity and allergic potential induced by topical application of triclosan in mice. Journal of immunotoxicology **13**, 165-172.10.3109/1547691x.2015.1029146

Arias-Cavieres, A., More, J., Vicente, J.M., Adasme, T., Hidalgo, J., Valdes, J.L., Humeres, A., Valdes-Undurraga, I., Sanchez, G., Hidalgo, C., Barrientos, G., 2018. Triclosan Impairs Hippocampal Synaptic Plasticity and Spatial Memory in Male Rats. Front Mol Neurosci **11**, 429.10.3389/fnmol.2018.00429

Barrandon, Y., Green, H., 1985. Cell size as a determinant of the clone-forming ability of human keratinocytes. Proc Natl Acad Sci U S A **82**, 5390-5394.10.1073/pnas.82.16.5390

Barros, S.P., Wirojchanasak, S., Barrow, D.A., Panagakos, F.S., Devizio, W., Offenbacher, S., 2010. Triclosan inhibition of acute and chronic inflammatory gene pathways. Journal of clinical periodontology **37**, 412-418.10.1111/j.1600-051X.2010.01548.x

Bean, B.P., 2007. The action potential in mammalian central neurons. Nature reviews. Neuroscience **8**, 451-465.10.1038/nrn2148

Beck, A., Fleig, A., Penner, R., Peinelt, C., 2014. Regulation of endogenous and heterologous Ca^{2+} release-activated Ca^{2+} currents by pH. Cell calcium **56**, 235-243.10.1016/j.ceca.2014.07.011

Berezhnov, A.V., Soutar, M.P., Fedotova, E.I., Frolova, M.S., Plun-Favreau, H., Zinchenko, V.P., Abramov, A.Y., 2016. Intracellular pH Modulates Autophagy and Mitophagy. J Biol Chem **291**, 8701-8708.10.1074/jbc.M115.691774

Bernauer, U., 2015 Opinion on Cetylpyridinium Chloride- Submission II (p97). Scientific Committee on Consumer Safety, SCCS/1548/15

Berridge, M.J., 1993. Inositol trisphosphate and calcium signalling. Nature **361**, 315-325.10.1038/361315a0

Bertorello, A.M., Komarova, Y., Smith, K., Leibiger, I.B., Efendiev, R., Pedemonte, C.H., Borisy, G., Sznajder, J.I., 2003. Analysis of Na+,K+-ATPase motion and incorporation into the plasma membrane in response to G protein-coupled receptor signals in living cells. Mol Biol Cell **14**, 1149-1157.10.1091/mbc.e02-06-0367

Bhandari, P., Song, M., Chen, Y., Burelle, Y., Dorn, G.W., 2nd, 2014. Mitochondrial contagion induced by Parkin deficiency in Drosophila hearts and its containment by suppressing mitofusin. Circulation research **114**, 257-265.10.1161/circresaha.114.302734

Binelli, A., Cogni, D., Parolini, M., Riva, C., Provini, A., 2009. In vivo experiments for the evaluation of genotoxic and cytotoxic effects of Triclosan in Zebra mussel hemocytes. Aquatic toxicology (Amsterdam, Netherlands) **91**, 238-244.10.1016/j.aquatox.2008.11.008

Blank, U., Essig, M., Scandiuzzi, L., Benhamou, M., Kanamaru, Y., 2007. Mast cells and inflammatory kidney disease. Immunol Rev **217**, 79-95.10.1111/j.1600-065X.2007.00503.x

Boron, W.F., 2004. Regulation of intracellular pH. Advances in physiology education **28**, 160-179.10.1152/advan.00045.2004

Borovinskaya, M.A., Shoji, S., Fredrick, K., Cate, J.H., 2008. Structural basis for hygromycin B inhibition of protein biosynthesis. RNA (New York, N.Y.) **14**, 1590-1599.10.1261/rna.1076908

Bronner, C., Mousli, M., Eleno, N., Landry, Y., 1989. Resting plasma membrane potential of rat peritoneal mast cells is set predominantly by the sodium pump. FEBS letters **255**, 401-404.10.1016/0014-5793(89)81132-9

Buckler, K.J., Vaughan-Jones, R.D., 1998. Effects of mitochondrial uncouplers on intracellular calcium, pH and membrane potential in rat carotid body type I cells. The Journal of physiology **513 (Pt 3)**, 819-833.10.1111/j.1469-7793.1998.819ba.x

Cai, S., Zhu, J., Sun, L., Fan, C., Zhong, Y., Shen, Q., Li, Y., 2019. Association Between Urinary Triclosan With Bone Mass Density and Osteoporosis in US Adult Women, 2005–2010. The Journal of clinical endocrinology and metabolism **104**, 4531-4538.10.1210/jc.2019-00576

Calafat, A.M., Ye, X., Wong, L.Y., Reidy, J.A., Needham, L.L., 2008. Urinary concentrations of triclosan in the U.S. population: 2003-2004. Environmental health perspectives **116**, 303-307.10.1289/ehp.10768

Chahdi, A., Choi, W.S., Kim, Y.M., Fraundorfer, P.F., Beaven, M.A., 2002. Serine/threonine protein kinases synergistically regulate phospholipase D1 and 2 and secretion in RBL-2H3 mast cells. Mol Immunol **38**, 1269-1276.10.1016/s0161-5890(02)00074-3

Chalfie, M., Kain, S., 2005. Green Fluorescent Protein: Properties, Applications and Protocols. John Wiley & Sons.

Chamberland, S., Yang, H.H., Pan, M.M., Evans, S.W., Guan, S., Chavarha, M., Yang, Y., Salesse, C., Wu, H., Wu, J.C., Clandinin, T.R., Toth, K., Lin, M.Z., St-Pierre, F., 2017. Fast two-photon imaging of subcellular voltage dynamics in neuronal tissue with genetically encoded indicators. Elife **6**, e25690.10.7554/eLife.25690

Chandra, S., Fewtrell, C., Millard, P.J., Sandison, D.R., Webb, W.W., Morrison, G.H., 1994. Imaging of total intracellular calcium and calcium influx and efflux in individual resting and stimulated tumor mast cells using ion microscopy. J Biol Chem **269**, 15186-15194

Chen, H., Detmer, S.A., Ewald, A.J., Griffin, E.E., Fraser, S.E., Chan, D.C., 2003. Mitofusins Mfn1 and Mfn2 coordinately regulate mitochondrial fusion and are essential for embryonic development. J Cell Biol **160**, 189-200.10.1083/jcb.200211046

Chen, T.W., Wardill, T.J., Sun, Y., Pulver, S.R., Renninger, S.L., Baohan, A., Schreiter, E.R., Kerr, R.A., Orger, M.B., Jayaraman, V., Looger, L.L., Svoboda, K., Kim, D.S., 2013. Ultrasensitive fluorescent proteins for imaging neuronal activity. Nature **499**, 295-300.10.1038/nature12354

Choi, J.J., Park, B.K., Park, S., Yun, C.Y., Kim, D.H., Kim, J.S., Hwang, E.S., Jin, M., 2009. Development of an in vitro test system measuring transcriptional downregulatory activities on IL-13. Journal of microbiology and biotechnology **19**, 331-337

Compan, V., Baroja-Mazo, A., López-Castejón, G., Gomez, A.I., Martínez, C.M., Angosto, D., Montero, M.T., Herranz, A.S., Bazán, E., Reimers, D., Mulero, V., Pelegrín, P., 2012. Cell volume regulation modulates NLRP3 inflammasome activation. Immunity **37**, 487-500.10.1016/j.immuni.2012.06.013

Cui, M., Tang, X., Christian, W.V., Yoon, Y., Tieu, K., 2010. Perturbations in mitochondrial dynamics induced by human mutant PINK1 can be rescued by the mitochondrial division inhibitor mdivi-1. J Biol Chem **285**, 11740-11752.10.1074/jbc.M109.066662

Curthoys, N.M., Mlodzianoski, M.J., Parent, M., Butler, M.B., Raut, P., Wallace, J., Lilieholm, J., Mehmood, K., Maginnis, M.S., Waters, H., Busse, B., Zimmerberg, J., Hess, S.T., 2019. Influenza Hemagglutinin Modulates Phosphatidylinositol 4,5-Bisphosphate Membrane Clustering. Biophys J **116**, 893-909.10.1016/j.bpj.2019.01.017

Daoud, F.C., Edmiston, C.E., Jr., Leaper, D., 2014. Meta-analysis of prevention of surgical site infections following incision closure with triclosan-coated sutures: robustness to new evidence. Surgical infections **15**, 165-181.10.1089/sur.2013.177

Datta, S., He, G., Tomilov, A., Sahdeo, S., Denison, M.S., Cortopassi, G., 2017. In Vitro Evaluation of Mitochondrial Function and Estrogen Signaling in Cell Lines Exposed to the Antiseptic Cetylpyridinium Chloride. Environmental health perspectives **125**, 087015.10.1289/ehp1404

Delrue, I., Pan, Q., Baczmanska, A.K., Callens, B.W., Verdoodt, L.L.M., 2018. Determination of the Selection Capacity of Antibiotics for Gene Selection. Biotechnology journal **13**, e1700747.10.1002/biot.201700747

Dvorak, A.M., 1986. Mast-cell degranulation in human hearts. The New England journal of medicine **315**, 969-970.10.1056/nejm198610093151515

Elieh-Ali-Komi, D., Cao, Y., 2017. Role of Mast Cells in the Pathogenesis of Multiple Sclerosis and Experimental Autoimmune Encephalomyelitis. Clinical reviews in allergy & immunology **52**, 436-445.10.1007/s12016-016-8595-y

Etzel, T.M., Calafat, A.M., Ye, X., Chen, A., Lanphear, B.P., Savitz, D.A., Yolton, K., Braun, J.M., 2017. Urinary triclosan concentrations during pregnancy and birth outcomes. Environmental research **156**, 505-511.10.1016/j.envres.2017.04.015

Farrell, D.J., Hines, J.E., Walls, A.F., Kelly, P.J., Bennett, M.K., Burt, A.D., 1995. Intrahepatic mast cells in chronic liver diseases. Hepatology (Baltimore, Md.) **22**, 1175-1181.10.1016/0270-9139(95)90627-4

Feske, S., 2007. Calcium signalling in lymphocyte activation and disease. Nature reviews. Immunology **7**, 690-702.10.1038/nri2152

Fewtrell, C., Geier, M., Goetze, A., Holowka, D., Isenman, D.E., Jones, J.F., Metzger, H., Navia, M., Sieckmann, D., Silverton, E., Stein, K., 1979. Mediation of effector functions by antibodies: report of a workshop. Mol Immunol **16**, 741-754.10.1016/0161-5890(79)90152-4

Furuno, T., Shinkai, N., Inoh, Y., Nakanishi, M., 2015. Impaired expression of the mitochondrial calcium uniporter suppresses mast cell degranulation. Molecular and cellular biochemistry **410**, 215-221.10.1007/s11010-015-2554-4

Galli, S.J., Kalesnikoff, J., Grimbaldeston, M.A., Piliponsky, A.M., Williams, C.M., Tsai, M., 2005. Mast cells as "tunable" effector and immunoregulatory cells: recent advances. Annual review of immunology **23**, 749-786.10.1146/annurev.immunol.21.120601.141025

Gentile, D.A., Skoner, D.P., 1996. A role for the sodium, potassium adenosine triphosphatase (Na+,K+ ATPase) enzyme in degranulation of rat basophilic leukaemia cells. Clinical and experimental allergy : journal of the British Society for Allergy and Clinical Immunology **26**, 1449-1460

Giedt, R.J., Pfeiffer, D.R., Matzavinos, A., Kao, C.Y., Alevriadou, B.R., 2012. Mitochondrial dynamics and motility inside living vascular endothelial cells: role of bioenergetics. Annals of biomedical engineering **40**, 1903-1916.10.1007/s10439-012-0568-6

Gilbert, R.J., 1987. The oral clearance of zinc and triclosan after delivery from a dentifrice. J Pharm Pharmacol **39**, 480-483.10.1111/j.2042-7158.1987.tb03425.x

Girolamo, F., Coppola, C., Ribatti, D., 2017. Immunoregulatory effect of mast cells influenced by microbes in neurodegenerative diseases. Brain, behavior, and immunity **65**, 68-89.10.1016/j.bbi.2017.06.017

Gottlieb, S., 2019.Federal register. Vol.**84 (71):** https://www.govinfo.gov/content/pkg/FR-2019-04-12/pdf/2019-06791.pdf

Gudheti, M.V., Curthoys, N.M., Gould, T.J., Kim, D., Gunewardene, M.S., Gabor, K.A., Gosse, J.A., Kim, C.H., Zimmerberg, J., Hess, S.T., 2013. Actin mediates the nanoscale membrane organization of the clustered membrane protein influenza hemagglutinin. Biophys J **104**, 2182-2192.10.1016/j.bpj.2013.03.054

Guillery, O., Malka, F., Frachon, P., Milea, D., Rojo, M., Lombès, A., 2008. Modulation of mitochondrial morphology by bioenergetics defects in primary human fibroblasts. Neuromuscular disorders : NMD **18**, 319-330.10.1016/j.nmd.2007.12.008

Guo, Z., Turner, C., Castle, D., 1998. Relocation of the t-SNARE SNAP-23 from lamellipodia-like cell surface projections regulates compound exocytosis in mast cells. Cell **94**, 537-548.10.1016/s0092-8674(00)81594-9

Gurskaya, N.G., Verkhusha, V.V., Shcheglov, A.S., Staroverov, D.B., Chepurnykh, T.V., Fradkov, A.F., Lukyanov, S., Lukyanov, K.A., 2006. Engineering of a monomeric green-to-red photoactivatable fluorescent protein induced by blue light. Nature biotechnology **24**, 461-465.10.1038/nbt1191

Hara, Y., Yuk, F., Puri, R., Janssen, W.G., Rapp, P.R., Morrison, J.H., 2014. Presynaptic mitochondrial morphology in monkey prefrontal cortex correlates with working memory and is improved with estrogen treatment. Proc Natl Acad Sci U S A **111**, 486-491.10.1073/pnas.1311310110

Hemalatha, D., Nataraj, B., Rangasamy, B., Shobana, C., Ramesh, M., 2019. DNA damage and physiological responses in an Indian major carp Labeo rohita exposed to an antimicrobial agent triclosan. Fish physiology and biochemistry **45**, 1463-1484.10.1007/s10695-019-00661-2

Hempel, H.A., Cuka, N.S., Kulac, I., Barber, J.R., Cornish, T.C., Platz, E.A., De Marzo, A.M., Sfanos, K.S., 2017. Low Intratumoral Mast Cells Are Associated With a Higher Risk of Prostate Cancer Recurrence. The Prostate **77**, 412-424.10.1002/pros.23280

Hess, S.T., Girirajan, T.P., Mason, M.D., 2006. Ultra-high resolution imaging by fluorescence photoactivation localization microscopy. Biophys J **91**, 4258-4272.10.1529/biophysj.106.091116

Hill-Eubanks, D.C., Werner, M.E., Heppner, T.J., Nelson, M.T., 2011. Calcium signaling in smooth muscle. Cold Spring Harbor perspectives in biology **3**, a004549.10.1101/cshperspect.a004549

Hogan, P.G., Lewis, R.S., Rao, A., 2010. Molecular basis of calcium signaling in lymphocytes: STIM and ORAI. Annual review of immunology **28**, 491-533.10.1146/annurev.immunol.021908.132550

Holowka, D., Calloway, N., Cohen, R., Gadi, D., Lee, J., Smith, N.L., Baird, B., 2012. Roles for ca(2+) mobilization and its regulation in mast cell functions. Front Immunol **3**, 104.10.3389/fimmu.2012.00104

Holowka, D., Thanapuasuwan, K., Baird, B., 2018. Short chain ceramides disrupt immunoreceptor signaling by inhibiting segregation of Lo from Ld Plasma membrane components. Biol Open **7**.10.1242/bio.034702

Huang, B., Wang, W., Bates, M., Zhuang, X., 2008. Three-dimensional super-resolution imaging by stochastic optical reconstruction microscopy. Science **319**, 810-813.10.1126/science.1153529

Hurd-Brown, T., Udoji, F., Martin, T., Whalen, M.M., 2013. Effects of DDT and triclosan on tumor-cell binding capacity and cell-surface protein expression of human natural killer cells. J Appl Toxicol **33**, 495-502.10.1002/jat.2767

Hutchinson, L.M., Trinh, B.M., Palmer, R.K., Preziosi, C.A., Pelletier, J.H., Nelson, H.M., Gosse, J.A., 2011. Inorganic arsenite inhibits IgE receptor-mediated degranulation of mast cells. J Appl Toxicol **31**, 231-241.10.1002/jat.1585

Jackson-Browne, M.S., Papandonatos, G.D., Chen, A., Calafat, A.M., Yolton, K., Lanphear, B.P., Braun, J.M., 2018. Identifying Vulnerable Periods of Neurotoxicity to Triclosan Exposure in Children. Environmental health perspectives **126**, 057001.10.1289/ehp2777

Jackson-Browne, M.S., Papandonatos, G.D., Chen, A., Yolton, K., Lanphear, B.P., Braun, J.M., 2019. Early-life triclosan exposure and parent-reported behavior problems in 8-year-old children. Environment international **128**, 446-456.10.1016/j.envint.2019.01.021

Jheng, H.F., Tsai, P.J., Guo, S.M., Kuo, L.H., Chang, C.S., Su, I.J., Chang, C.R., Tsai, Y.S., 2012. Mitochondrial fission contributes to mitochondrial dysfunction and insulin resistance in skeletal muscle. Molecular and cellular biology **32**, 309-319.10.1128/mcb.05603-11

Jin, L., Han, Z., Platisa, J., Wooltorton, J.R., Cohen, L.B., Pieribone, V.A., 2012. Single action potentials and subthreshold electrical events imaged in neurons with a fluorescent protein voltage probe. Neuron **75**, 779-785.10.1016/j.neuron.2012.06.040

Johnson, D., Nehrke, K., 2010. Mitochondrial fragmentation leads to intracellular acidification in Caenorhabditis elegans and mammalian cells. Mol Biol Cell **21**, 2191-2201.10.1091/mbc.e09-10-0874

Johnson, R.G., Carty, S.E., Fingerhood, B.J., Scarpa, A., 1980. The internal pH of mast cell granules. FEBS letters **120**, 75-79.10.1016/0014-5793(80)81050-7

Johnzon, C.F., Rönnberg, E., Pejler, G., 2016. The Role of Mast Cells in Bacterial Infection. The American journal of pathology **186**, 4-14.10.1016/j.ajpath.2015.06.024

Jurewicz, J., Radwan, M., Wielgomas, B., Kałużny, P., Klimowska, A., Radwan, P., Hanke, W., 2018. Environmental levels of triclosan and male fertility. Environmental science and pollution research international **25**, 5484-5490.10.1007/s11356-017-0866-5

Kary, T., 2019. Colgate Total Toothpaste to Relaunch Without Controversial Chemical. Bloomberg. June 19, 2020,https://www.bloomberg.com/news/articles/2019-01-15/colgate-total-toothpaste-to-relaunch-this-time-sans-triclosan

Kaufman, D.S., Goligorsky, M.S., Nord, E.P., Graber, M.L., 1993. Perturbation of cell pH regulation by H2O2 in renal epithelial cells. Archives of biochemistry and biophysics **302**, 245-254.10.1006/abbi.1993.1206

Kim, J., Kim, K., 2019. Association of antimicrobial household exposure with development of allergic rhinitis in Korea. Pediatric allergy and immunology : official publication of the European Society of Pediatric Allergy and Immunology **30**, 569-571.10.1111/pai.13052

Kinet, J.P., 1999. The high-affinity IgE receptor (Fc epsilon RI): from physiology to pathology. Annual review of immunology **17**, 931-972.10.1146/annurev.immunol.17.1.931

Koeppe, E.S., Ferguson, K.K., Colacino, J.A., Meeker, J.D., 2013. Relationship between urinary triclosan and paraben concentrations and serum thyroid measures in NHANES 2007-2008. The Science of the total environment **445-446**, 299-305.10.1016/j.scitotenv.2012.12.052

Koivusalo, M., Welch, C., Hayashi, H., Scott, C.C., Kim, M., Alexander, T., Touret, N., Hahn, K.M., Grinstein, S., 2010. Amiloride inhibits macropinocytosis by lowering submembranous pH and preventing Rac1 and Cdc42 signaling. J Cell Biol **188**, 547-563.10.1083/jcb.200908086

Kostyuk, A.I., Demidovich, A.D., Kotova, D.A., Belousov, V.V., Bilan, D.S., 2019. Circularly Permuted Fluorescent Protein-Based Indicators: History, Principles, and Classification. International journal of molecular sciences **20**, 4200.10.3390/ijms20174200

Kux, L., 2016a.Federal register. Vol.**81 (172): https://www.govinfo.gov/content/pkg/FR-2016-09-06/pdf/2016-21337.pdf**

Kux, L., 2016b.Federal register. Vol.**81 (126): https://www.govinfo.gov/content/pkg/FR-2016-06-30/pdf/2016-15410.pdf**

Kux, L., 2017.Federal register. Vol.**82 (243): https://www.govinfo.gov/content/pkg/FR-2017-12-20/pdf/2017-27317.pdf**

Kux, L., 2019.Federal register. Vol.**84 (71): https://www.govinfo.gov/content/pkg/FR-2019-04-12/pdf/2019-06791.pdf**

Lee, J., Veatch, S.L., Baird, B., Holowka, D., 2012. Molecular mechanisms of spontaneous and directed mast cell motility. J Leukoc Biol **92**, 1029-1041.10.1189/jlb.0212091

Lindau, M., Fernandez, J.M., 1986. A patch-clamp study of histamine-secreting cells. J Gen Physiol **88**, 349-368.10.1085/jgp.88.3.349

Lioudyno, M.I., Kozak, J.A., Penna, A., Safrina, O., Zhang, S.L., Sen, D., Roos, J., Stauderman, K.A., Cahalan, M.D., 2008. Orai1 and STIM1 move to the immunological synapse and are up-regulated during T cell activation. Proc Natl Acad Sci U S A **105**, 2011-2016.10.1073/pnas.0706122105

Lodish, H., Berk, A., Zipursky, S.L., Matsudaira, P., Baltimore, D., Darnell, J., 2000. Molecular Cell Biology, 4th ed. W.H. Freeman.

Luby-Phelps, K., 2000. Cytoarchitecture and physical properties of cytoplasm: volume, viscosity, diffusion, intracellular surface area. International review of cytology **192**, 189-221.10.1016/s0074-7696(08)60527-6

Lv, Y., Rui, C., Dai, Y., Pang, Q., Li, Y., Fan, R., Lu, S., 2016. Exposure of children to BPA through dust and the association of urinary BPA and triclosan with oxidative stress in Guangzhou, China. Environmental science. Processes & impacts **18**, 1492-1499.10.1039/c6em00472e

Mahon, M.J., 2011. pHluorin2: an enhanced, ratiometric, pH-sensitive green florescent protein. Advances in bioscience and biotechnology (Print) **2**, 132-137.10.4236/abb.2011.23021

Mancarella, S., Wang, Y., Deng, X., Landesberg, G., Scalia, R., Panettieri, R.A., Mallilankaraman, K., Tang, X.D., Madesh, M., Gill, D.L., 2011. Hypoxia-induced acidosis uncouples the STIM-Orai calcium signaling complex. J Biol Chem **286**, 44788-44798.10.1074/jbc.M111.303081

Marano, N., Liotta, M.A., Slattery, J.P., Holowka, D., Baird, B., 1993. Fc epsilon RI and the T cell receptor for antigen activate similar signalling pathways in T cell-RBL cell hybrids. Cell Signal **5**, 155-167.10.1016/0898-6568(93)90067-v

Marshall, N.B., Lukomska, E., Long, C.M., Kashon, M.L., Sharpnack, D.D., Nayak, A.P., Anderson, K.L., Jean Meade, B., Anderson, S.E., 2015. Triclosan Induces Thymic Stromal Lymphopoietin in Skin Promoting Th2 Allergic Responses. Toxicol Sci **147**, 127-139.10.1093/toxsci/kfv113

Marshall, N.B., Lukomska, E., Nayak, A.P., Long, C.M., Hettick, J.M., Anderson, S.E., 2017. Topical application of the anti-microbial chemical triclosan induces immunomodulatory responses through the S100A8/A9-TLR4 pathway. Journal of immunotoxicology **14**, 50-59.10.1080/1547691x.2016.1258094

McLaughlin, S.G., Dilger, J.P., 1980. Transport of protons across membranes by weak acids. Physiological reviews **60**, 825-863.10.1152/physrev.1980.60.3.825

Metcalfe, D.D., Baram, D., Mekori, Y.A., 1997. Mast cells. Physiological reviews **77**, 1033-1079.10.1152/physrev.1997.77.4.1033

Metzger, H., Goetze, A., Kanellopoulos, J., Holowka, D., Fewtrell, C., 1982. Structure of the high-affinity mast cell receptor for IgE. Fed Proc **41**, 8-11

Millard, P.J., Gross, D., Webb, W.W., Fewtrell, C., 1988. Imaging asynchronous changes in intracellular Ca2+ in individual stimulated tumor mast cells. Proc Natl Acad Sci U S A **85**, 1854-1858.10.1073/pnas.85.6.1854

Miyawaki, A., Niino, Y., 2015. Molecular spies for bioimaging--fluorescent protein-based probes. Molecular cell **58**, 632-643.10.1016/j.molcel.2015.03.002

Mohr, F.C., Fewtrell, C., 1987a. Depolarization of rat basophilic leukemia cells inhibits calcium uptake and exocytosis. J Cell Biol **104**, 783-792.10.1083/jcb.104.3.783

Mohr, F.C., Fewtrell, C., 1987b. The relative contributions of extracellular and intracellular calcium to secretion from tumor mast cells. Multiple effects of the proton ionophore carbonyl cyanide m-chlorophenylhydrazone. J Biol Chem **262**, 10638-10643

Moss, T., Howes, D., Williams, F.M., 2000. Percutaneous penetration and dermal metabolism of triclosan (2,4, 4'-trichloro-2'-hydroxydiphenyl ether). Food and chemical toxicology : an international journal published for the British Industrial Biological Research Association **38**, 361-370.10.1016/s0278-6915(99)00164-7

Myers, V.B., Haydon, D.A., 1972. Ion transfer across lipid membranes in the presence of gramicidin A. II. The ion selectivity. Biochim Biophys Acta **274**, 313-322.10.1016/0005-2736(72)90179-4

Nakamura, U., Iwase, M., Uchizono, Y., Sonoki, K., Sasaki, N., Imoto, H., Goto, D., Iida, M., 2006. Rapid intracellular acidification and cell death by H2O2 and alloxan in pancreatic beta cells. Free radical biology & medicine **40**, 2047-2055.10.1016/j.freeradbiomed.2006.01.038

Nelson, D.L., Cox, M.M., 2017. Lehninger Principles of Biochemistry, 7th ed. W.H. Freeman.

Ouyang, F., Tang, N., Zhang, H.J., Wang, X., Zhao, S., Wang, W., Zhang, J., Cheng, W., 2018. Maternal urinary triclosan level, gestational diabetes mellitus and birth weight in Chinese women. The Science of the total environment **626**, 451-457.10.1016/j.scitotenv.2018.01.102

Ozawa, K., Yamada, K., Kazanietz, M.G., Blumberg, P.M., Beaven, M.A., 1993. Different isozymes of protein kinase C mediate feedback inhibition of phospholipase C and stimulatory signals for exocytosis in rat RBL-2H3 cells. J Biol Chem **268**, 2280-2283

Palmer, R.K., Hutchinson, L.M., Burpee, B.T., Tupper, E.J., Pelletier, J.H., Kormendy, Z., Hopke, A.R., Malay, E.T., Evans, B.L., Velez, A., Gosse, J.A., 2012. Antibacterial agent triclosan suppresses RBL-2H3 mast cell function. Toxicol Appl Pharmacol **258**, 99-108.10.1016/j.taap.2011.10.012

Parent, M., Hess, S.T., 2019. Quantification of Mitochondrial Membrane Curvature by Three-Dimensional Localization Microscopy. iScience Notes **4**.10.22580

Popova, L.B., Nosikova, E.S., Kotova, E.A., Tarasova, E.O., Nazarov, P.A., Khailova, L.S., Balezina, O.P., Antonenko, Y.N., 2018. Protonophoric action of triclosan causes calcium efflux from mitochondria, plasma membrane depolarization and bursts of miniature end-plate potentials. Biochim Biophys Acta Biomembr **1860**, 1000-1007.10.1016/j.bbamem.2018.01.008

Prakriya, M., Lewis, R.S., 2015. Store-Operated Calcium Channels. Physiological reviews **95**, 1383-1436.10.1152/physrev.00020.2014

Punt, J., Stranford, S., Jones, P., Owen, J., 2019. Kuby Immunology, 8th ed. W.H. Freeman.

Putney, J.W., Jr., 1986. A model for receptor-regulated calcium entry. Cell calcium **7**, 1-12.10.1016/0143-4160(86)90026-6

Queckenberg, C., Meins, J., Wachall, B., Doroshyenko, O., Tomalik-Scharte, D., Bastian, B., Abdel-Tawab, M., Fuhr, U., 2010. Absorption, pharmacokinetics, and safety of triclosan after dermal administration. Antimicrob Agents Chemother **54**, 570-572.10.1128/aac.00615-09

Riva, C., Cristoni, S., Binelli, A., 2012. Effects of triclosan in the freshwater mussel Dreissena polymorpha: a proteomic investigation. Aquatic toxicology (Amsterdam, Netherlands) **118-119**, 62-71.10.1016/j.aquatox.2012.03.013

Rover, J.A., Leu-Wai-See, P., 2014. Role of Colgate Total toothpaste in helping control plaque and gingivitis. American journal of dentistry **27**, 167-170

Safiulina, D., Veksler, V., Zharkovsky, A., Kaasik, A., 2006. Loss of mitochondrial membrane potential is associated with increase in mitochondrial volume: physiological role in neurones. J Cell Physiol **206**, 347-353.10.1002/jcp.20476

Sarkadi, B., Tordai, A., Gardos, G., 1990. Membrane depolarization selectively inhibits receptor-operated calcium channels in human T (Jurkat) lymphoblasts. Biochim Biophys Acta **1027**, 130-140.10.1016/0005-2736(90)90076-z

Schurr, A., 2014. Cerebral glycolysis: a century of persistent misunderstanding and misconception. Frontiers in neuroscience **8**, 360.10.3389/fnins.2014.00360

Seldin, D.C., Adelman, S., Austen, K.F., Stevens, R.L., Hein, A., Caulfield, J.P., Woodbury, R.G., 1985. Homology of the rat basophilic leukemia cell and the rat mucosal mast cell. Proc Natl Acad Sci U S A **82**, 3871-3875.10.1073/pnas.82.11.3871

Shim, J., Weatherly, L.M., Luc, R.H., Dorman, M.T., Neilson, A., Ng, R., Kim, C.H., Millard, P.J., Gosse, J.A., 2016. Triclosan is a mitochondrial uncoupler in live zebrafish. J Appl Toxicol **36**, 1662-1667.10.1002/jat.3311

Shim, J.K., Caron, M.A., Weatherly, L.M., Gerchman, L.B., Sangroula, S., Hattab, S., Baez, A.Y., Briana, T.J., Gosse, J.A., 2019. Antimicrobial agent triclosan suppresses mast cell signaling via phospholipase D inhibition. J Appl Toxicol **39**, 1672-1690.10.1002/jat.3884

Silver, R., Curley, J.P., 2013. Mast cells on the mind: new insights and opportunities. Trends in neurosciences **36**, 513-521.10.1016/j.tins.2013.06.001

Smith, A.J., Pfeiffer, J.R., Zhang, J., Martinez, A.M., Griffiths, G.M., Wilson, B.S., 2003. Microtubule-dependent transport of secretory vesicles in RBL-2H3 cells. Traffic **4**, 302-312.10.1034/j.1600-0854.2003.00084.x

Sneath, P.H., 1957. The application of computers to taxonomy. Journal of general microbiology **17**, 201-226.10.1099/00221287-17-1-201

Sporik, R., Kemp, A.S., 1997. Topical triclosan treatment of atopic dermatitis. The Journal of allergy and clinical immunology **99**, 861.10.1016/s0091-6749(97)80029-2

Stawicki, T.M., Owens, K.N., Linbo, T., Reinhart, K.E., Rubel, E.W., Raible, D.W., 2014. The zebrafish merovingian mutant reveals a role for pH regulation in hair cell toxicity and function. Disease models & mechanisms **7**, 847-856.10.1242/dmm.016576

Stepanenko, O.V., Verkhusha, V.V., Kuznetsova, I.M., Uversky, V.N., Turoverov, K.K., 2008. Fluorescent proteins as biomarkers and biosensors: throwing color lights on molecular and cellular processes. Current protein & peptide science **9**, 338-369.10.2174/138920308785132668

Takekawa, M., Furuno, T., Hirashima, N., Nakanishi, M., 2012. Mitochondria take up Ca2+ in two steps dependently on store-operated Ca2+ entry in mast cells. Biological & pharmaceutical bulletin **35**, 1354-1360.10.1248/bpb.b110576

Tamura, I., Kanbara, Y., Saito, M., Horimoto, K., Satoh, M., Yamamoto, H., Oyama, Y., 2012. Triclosan, an antibacterial agent, increases intracellular Zn(2+) concentration in rat thymocytes: its relation to oxidative stress. Chemosphere **86**, 70-75.10.1016/j.chemosphere.2011.09.009

Tan, W.P., Suresh, S., Tey, H.L., Chiam, L.Y., Goon, A.T., 2010. A randomized double-blind controlled trial to compare a triclosan-containing emollient with vehicle for the treatment of atopic dermatitis. Clinical and experimental dermatology **35**, e109-112.10.1111/j.1365-2230.2009.03719.x

Tantama, M., Hung, Y.P., Yellen, G., 2011. Imaging intracellular pH in live cells with a genetically encoded red fluorescent protein sensor. J Am Chem Soc **133**, 10034-10037.10.1021/ja202902d

Te Winkel, J.D., Gray, D.A., Seistrup, K.H., Hamoen, L.W., Strahl, H., 2016. Analysis of Antimicrobial-Triggered Membrane Depolarization Using Voltage Sensitive Dyes. Front Cell Dev Biol **4**, 29.10.3389/fcell.2016.00029

Theoharides, T.C., Sant, G.R., 1991. Bladder mast cell activation in interstitial cystitis. Seminars in urology **9**, 74-87

Thompson, M.A., Pabelick, C.M., Prakash, Y.S., 2009. Role of STIM1 in regulation of store-operated Ca2+ influx in pheochromocytoma cells. Cellular and molecular neurobiology **29**, 193-202.10.1007/s10571-008-9311-0

Thrasher, S.M., Scalfone, L.K., Holowka, D., Appleton, J.A., 2013. In vitro modelling of rat mucosal mast cell function in Trichinella spiralis infection. Parasite Immunol **35**, 21-31.10.1111/pim.12014

Trebak, M., Kinet, J.P., 2019. Calcium signalling in T cells. Nature reviews. Immunology **19**, 154-169.10.1038/s41577-018-0110-7

Tretter, L., Chinopoulos, C., Adam-Vizi, V., 1998. Plasma membrane depolarization and disturbed Na+ homeostasis induced by the protonophore carbonyl cyanide-p-trifluoromethoxyphenyl-hydrazon in isolated nerve terminals. Mol Pharmacol **53**, 734-741.10.1124/mol.53.4.734

Tsujikawa, H., Yu, A.S., Xie, J., Yue, Z., Yang, W., He, Y., Yue, L., 2015. Identification of key amino acid residues responsible for internal and external pH sensitivity of Orai1/STIM1 channels. Sci Rep **5**, 16747.10.1038/srep16747

Tsukioka, M., Iino, M., Endo, M., 1994. pH dependence of inositol 1,4,5-trisphosphate-induced Ca2+ release in permeabilized smooth muscle cells of the guinea-pig. The Journal of physiology **475**, 369-375.10.1113/jphysiol.1994.sp020078

Udoji, F., Martin, T., Etherton, R., Whalen, M.M., 2010. Immunosuppressive effects of triclosan, nonylphenol, and DDT on human natural killer cells in vitro. Journal of immunotoxicology **7**, 205-212.10.3109/15476911003667470

Vélez, M.P., Arbuckle, T.E., Fraser, W.D., 2015. Female exposure to phenols and phthalates and time to pregnancy: the Maternal-Infant Research on Environmental Chemicals (MIREC) Study. Fertility and sterility **103**, 1011-1020.e1012.10.1016/j.fertnstert.2015.01.005

Vig, M., Beck, A., Billingsley, J.M., Lis, A., Parvez, S., Peinelt, C., Koomoa, D.L., Soboloff, J., Gill, D.L., Fleig, A., Kinet, J.P., Penner, R., 2006. CRACM1 multimers form the ion-selective pore of the CRAC channel. Current biology : CB **16**, 2073-2079.10.1016/j.cub.2006.08.085

Wang, L., Izadmehr, S., Kamau, E., Kong, X.P., Chen, B.K., 2019. Sequential trafficking of Env and Gag to HIV-1 T cell virological synapses revealed by live imaging. Retrovirology **16**, 2.10.1186/s12977-019-0464-3

Wang, X., Chen, X., Feng, X., Chang, F., Chen, M., Xia, Y., Chen, L., 2015. Triclosan causes spontaneous abortion accompanied by decline of estrogen sulfotransferase activity in humans and mice. Sci Rep **5**, 18252.10.1038/srep18252

Wang, X., Ouyang, F., Feng, L., Wang, X., Liu, Z., Zhang, J., 2017. Maternal Urinary Triclosan Concentration in Relation to Maternal and Neonatal Thyroid Hormone Levels: A Prospective Study. Environmental health perspectives **125**, 067017.10.1289/ehp500

Weatherly, L.M.Molecular Mechanisms Underlying Effects of Antibacterial Agent Triclosan on Cellular Signal Transduction and Mitochondrial Function(2017). *Electronic Theses and Dissertations* https://digitalcommons.library.umaine.edu/etd/2727/

Weatherly, L.M., Gosse, J.A., 2017. Triclosan exposure, transformation, and human health effects. Journal of toxicology and environmental health. Part B, Critical reviews **20**, 447-469.10.1080/10937404.2017.1399306

Weatherly, L.M., Kennedy, R.H., Shim, J., Gosse, J.A., 2013. A microplate assay to assess chemical effects on RBL-2H3 mast cell degranulation: effects of triclosan without use of an organic solvent. Journal of visualized experiments : JoVE, e50671.10.3791/50671

Weatherly, L.M., Nelson, A.J., Shim, J., Riitano, A.M., Gerson, E.D., Hart, A.J., de Juan-Sanz, J., Ryan, T.A., Sher, R., Hess, S.T., Gosse, J.A., 2018. Antimicrobial agent triclosan disrupts mitochondrial structure, revealed by super-resolution microscopy, and inhibits mast cell signaling via calcium modulation. Toxicol Appl Pharmacol **349**, 39-54.10.1016/j.taap.2018.04.005

Weatherly, L.M., Shane, H.L., Friend, S.A., Lukomska, E., Baur, R., Anderson, S.E., 2020. Topical application of the antimicrobial agent triclosan induces NLRP3 inflammasome activation and mitochondrial dysfunction. Toxicol Sci.10.1093/toxsci/kfaa056

Weatherly, L.M., Shim, J., Hashmi, H.N., Kennedy, R.H., Hess, S.T., Gosse, J.A., 2016. Antimicrobial agent triclosan is a proton ionophore uncoupler of mitochondria in living rat and human mast cells and in primary human keratinocytes. J Appl Toxicol **36**, 777-789.10.1002/jat.3209

Wischmeyer, E., Lentes, K.U., Karschin, A., 1995. Physiological and molecular characterization of an IRK-type inward rectifier K+ channel in a tumour mast cell line. Pflugers Arch **429**, 809-819

Xie, X., Lu, C., Wu, M., Liang, J., Ying, Y., Liu, K., Huang, X., Zheng, S., Du, X., Liu, D., Wen, Z., Hao, G., Yang, G., Feng, L., Jing, C., 2020. Association between triclocarban and triclosan exposures and the risks of type 2 diabetes mellitus and impaired glucose tolerance in the National Health and Nutrition Examination Survey (NHANES 2013-2014). Environment international **136**, 105445.10.1016/j.envint.2019.105445

Yueh, M.F., Taniguchi, K., Chen, S., Evans, R.M., Hammock, B.D., Karin, M., Tukey, R.H., 2014. The commonly used antimicrobial additive triclosan is a liver tumor promoter. Proc Natl Acad Sci U S A **111**, 17200-17205.10.1073/pnas.1419119111

Zaitsu, M., Narita, S., Lambert, K.C., Grady, J.J., Estes, D.M., Curran, E.M., Brooks, E.G., Watson, C.S., Goldblum, R.M., Midoro-Horiuti, T., 2007. Estradiol activates mast cells via a non-genomic estrogen receptor-alpha and calcium influx. Mol Immunol **44**, 1977-1985.10.1016/j.molimm.2006.09.030

Zamkowska, D., Karwacka, A., Jurewicz, J., Radwan, M., 2018. Environmental exposure to non-persistent endocrine disrupting chemicals and semen quality: An overview of the current epidemiological evidence. International journal of occupational medicine and environmental health **31**, 377-414.10.13075/ijomeh.1896.01195

Zhu, W., Zhou, W., Huo, X., Zhao, S., Gan, Y., Wang, B., Cheng, W., Ouyang, F., Wang, W., Tian, Y., Zhang, J., 2019. Triclosan and Female Reproductive Health: A Preconceptional Cohort Study. Epidemiology (Cambridge, Mass.) **30 Suppl 1**, S24-s31.10.1097/ede.0000000000001011

APPENDIX A

SUPPLEMENTARY INFORMATION TO CHAPTERS 2 & 3

Section A.1. Super-Resolution Imaging. FPALM imaging was done as published previously (Hess *et al.*, 2006; Gudheti *et al.*, 2013; Parent and Hess, 2019). Briefly, a 558 nm laser was focused into the back aperture of a 60× Olympus oil objective (1.45 NA) by a 350 mm lens (Thorlabs). The laser power out of the objective was ~9 mW. Fluorescence emission from Dendra2 was collected by the objective and filtered through a quad band dichroic (Di01-R405/488/561/635-25x36, Semrock, Rochester, NY) and 561 notch filter (NF03-561E-25, Semrock) to remove the laser and through final emission band pass filter (558/40 nm). A cylindrical lens of focal length 1000 mm was placed in the emission path to create astigmatism (Huang *et al.*, 2008). Two achromatic lenses of focal lengths +200 mm and +400 mm ware also added in the emission path for additional magnification. Fluorescence reaching the camera (iXon+ DU897DCS-BV, Andor Scientific, Dublin, Ireland), was recorded at a frequency of ~32 Hz with EM gain of 200. Transfected cells were chosen by observing the green (inactive) state of Dendra2 when excited by the light from the mercury lamp filtered by a narrow excitation bandpass filter (476/10nm, Chroma Technology, Inc., Bellows Falls, VT) and then imaged in epi-fluorescence mode using a band pass filter (535/50 M, Chroma Technology) before viewing through eyepieces or with the camera (EM gain disabled). After selecting a transfected cell, it was imaged for 10000 frames. A weak intensity of 405 nm light (a few microwatts total power) was used to illuminate the cell and photoactivate inactive Dendra2 to its active form (Gurskaya *et al.*, 2006).

Section A.2 Axial Position Calibration Procedure. For determination of the calibration between the axial position and observed astigmatism, fluorescent beads were imaged with a specific procedure. The objective was mounted on piezoelectric axial focus collar (Physik Instrumente (PI), Karlsruhe, Germany, PD72Z1x) which controlled the axial movement of the objective relative to the sample. Beads of diameter 0.1μm (Tetraspeck Microspheres, Thermofisher) plated in the Nunc 8 well chamber were imaged at ten different axial positions of the objective at a frame rate of ~32 Hz for 50 frames. The step size between each axial position of the objective was 200 nm and was controlled by PI MicroMove software. Each PSF, whose x and y radii are dependent on the position of the fluorophore, was fitted to localize the beads, and determine its distance below or above the focal plane. Calibration curves were obtained by plotting and analyzing the x and y radius as a function of axial position (Parent and Hess, 2019).

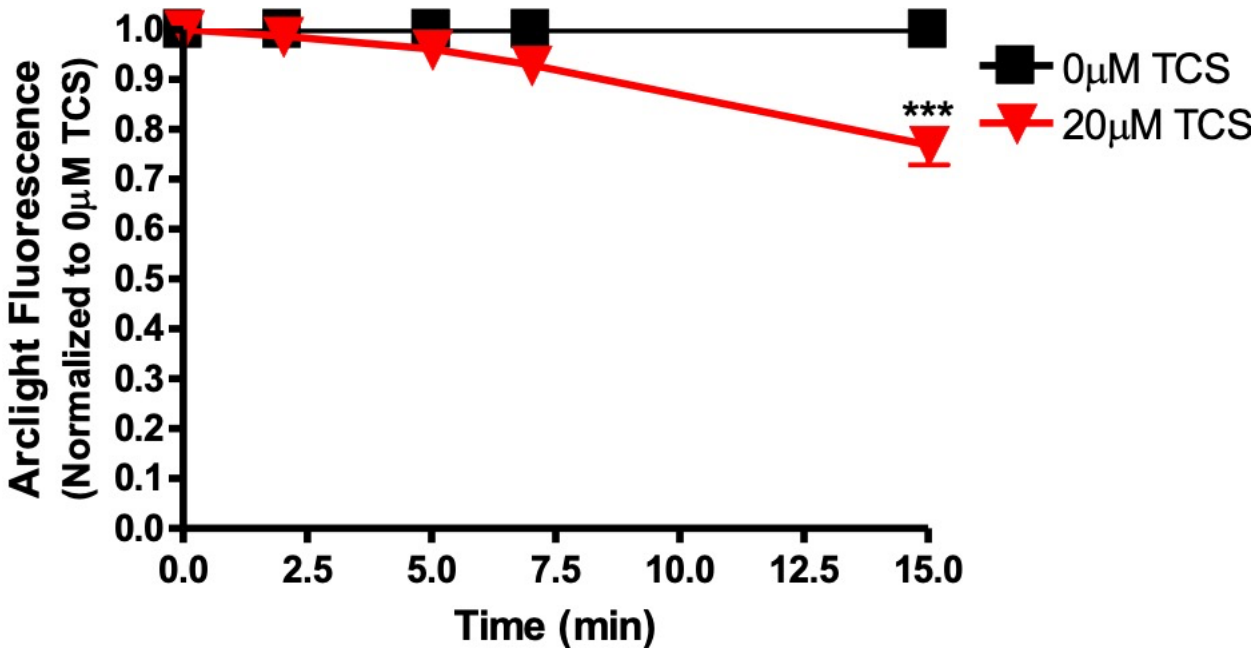

Figure A.3. Triclosan effects on the fluorescence of Arclight-242 in RBL-2H3 mast cells when measured through automated image analysis. Confocal image data from Figure 3.3 for control (0 μM) and 20 μM TCS were reanalyzed and processed using automated image analysis described in the "Automated Image Analysis" in Chapter 2. Triclosan depresses ArcLight-A242 fluorescence; these results are quantitatively similar to those obtained with the manual image analysis method in Figure 3.3B. Values presented are means ± SEM of at least 3 independent days of experiments per treatment. Statistically significant results, as compared to the control (0μM TCS), are represented by ***p value< 0.001, as determined by one-way ANOVA followed by Tukey's post-hoc test.

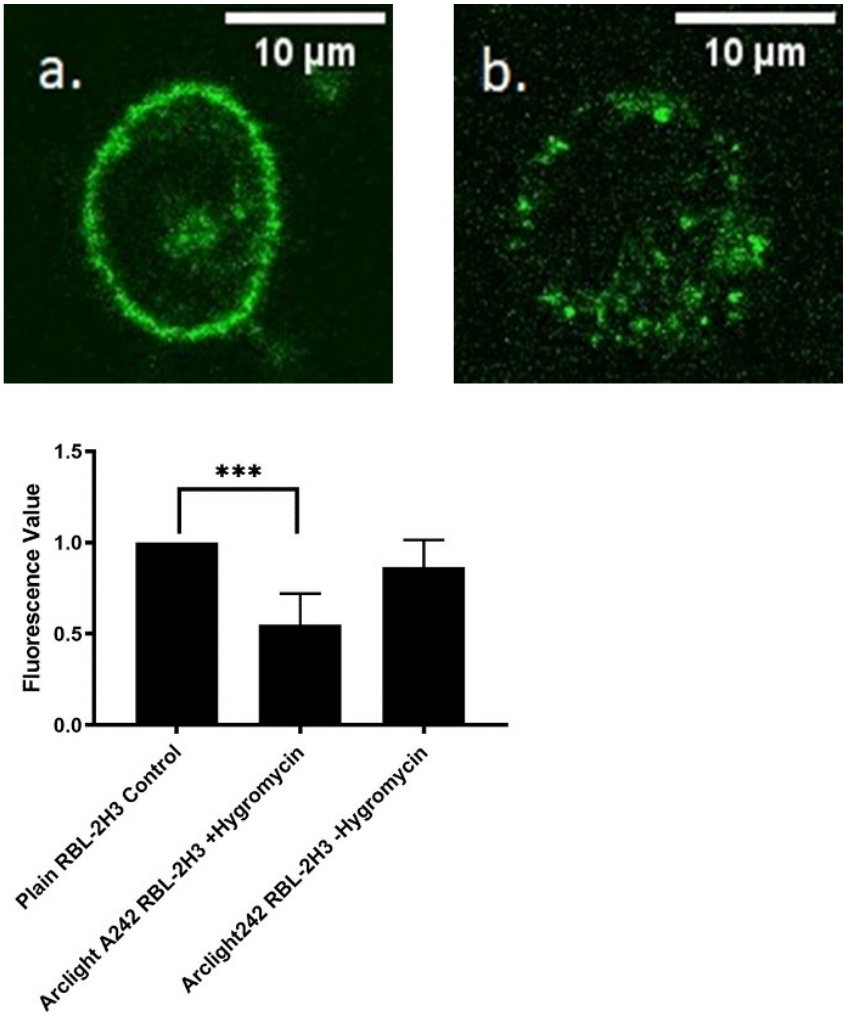

Figure A.4. **Production, screening and fluorescence measurement of ArcLight-A242 RBL stably-transfected clones.**

Creation of an ArcLight-A242 stably-transfected, high-expressing, clonal RBL-2H3 mast cell line would be useful for rapid, high-throughput studies of toxicant and drug effects on plasma membrane potential, at various doses and timeframes. Previously, we had attempted to measure Arclight fluorescence in transiently-transfected RBL-2H3 cells via plate reader, but the relatively low transfection rate resulted in insufficient fluorescence signal.

Methods for (A) and (B): Production and Screening of ArcLight-A242 RBL Cell Stably-transfected Clones. RBL-2H3 mast cells were maintained and transfected with ArcLight-A242 as described in Chapter 2. Immediately following electroporation, the 100 µL cell sample was combined with 500 µL pre-warmed, phenol red-containing RBL media, mixed gently, and placed into a well of a sterile, tissue culture-treated 6-well plate containing 1.5 mL media for overnight incubation at 37°C/5% CO_2. The next day, cells were trypsinized, centrifuged, and reconstituted to 1 x 10^6 cells/mL before serial dilution into 100 mm sterile, tissue culture-treated dishes, each

containing 7 mL of phenol red-containing RBL media (Hutchinson *et al.*, 2011) and a cell count between 100 and 100,000 cells (cell number varied to optimize both cell growth and clonal dilution; densities that gave the best results were 100 and 500 cells per well). The next day, media was removed from each dish and was replaced with 500 µg/mL hygromycin- and phenol red-containing RBL media. Hygromycin was used because the ArcLight-A242 construct contains a hygromycin-resistance gene (ArcLight-A242, a gift from Vincent Pieribone; Addgene plasmid # 36857; http://n2t.net/addgene:36857; RRID:Addgene_36857) (Jin *et al.*, 2012) . While a previous RBL transfection study with a different hygromycin-resistant construct employed 400 µg/mL hygromycin (Choi *et al.*, 2009), a dose-response killing curve was conducted with untransfected RBL cells, testing from 200 µg/ml to 1000 µg/ml, to determine the optimal concentration (Delrue *et al.*, 2018). While the dry hygromycin solid is stable for at least 5 years at 2-8°C, hygromycin is stable at 37°C for 30 days when dissolved in aqueous solutions (Sigma Aldrich), thus allowing the extended cultures needed for clonal selection. Non-toxic selective efficiency was optimized at 500 µg/mL (data not shown). Approximately 7 to 10 days later, separated colonies became visible. Media was discarded, 100 mm dishes were washed twice with RBL media which was then removed. Media-dipped calcium alginate fiber-tipped wood applicator swabs (Fisher Scientific) were used to pick individual colonies, these hygromycin-resistant transfectants were plated in 12-well plates (each well containing one colony and 1.5 mL of 500 µg/mL hygromycin- and phenol red-containing RBL media). Following a wash into fresh hygromycin media the next day, the clones were maintained for a week. When confluent, cells were harvested via 0.5 mL/well trypsinization, then transferred directly to 6-well plates, each containing 2.5 mL fresh hygromycin RBL media. After a few days, the cells were harvested via 1 mL/well trypsinization, quenched with 4 mL RBL media, centrifuged, counted, and brought to $1x10^6$ cells/mL in phenol red-free RBL media. A portion of each of these cell mixtures (100 µL) was combined with 100 µL phenol red-free RBL media and placed into a well of an ibidi 8-well plate and grown overnight at 37°C/5% for next-day screening (see below). The remainder of each clone was cultured in a 37 °C and 5% CO_2 incubator in a T25 flask in hygromycin- and phenol red-containing media. The next day, ibidi wells were washed with BT and images were taken in the presence of 200 µL BT per well. Confocal settings for ArcLight-A242 imaging are described in Chapter 2.

Results for (A) and (B): Confocal fluorescence images of RBL-2H3 cells transiently (A) or stably (B) expressing ArcLight-A242 show uniform localization of ArcLight at the plasma membrane following transient transfection (A; also Fig. 3A) but irregular intracellular distribution and aggregation of ArcLight in stably-transfected cells (B). Stable transfectants display aggregation of the construct as well as poor localization at the plasma membrane, compromising their viability in plasma membrane polarity assays (**B**).

In order to determine whether these stable transfectants possess sufficient fluorescence signal for high-throughput plate reader experiments, Arclight fluorescence was measured in a plate reader and compared to that of untransfected cells.

Methods For (C): Plate reader fluorescence measurements of stably-transfected ArcLight-A242 RBL-2H3 mast cells. A clone of ArcLight stably-transfected cells was split into two flasks and cultured for one week in phenol red-containing RBL media, one with and one without 500 µg/mL hygromycin. A day prior to the experiment, all media were replaced with phenol red-free media, including a flask of control untransfected RBL cells. On the day of the experiment,

cells were harvested using cell harvest buffer (Shim *et al.*, 2019) and plated in a Grenier 96-well clear flat bottom plate at densities of 150,000 cells/well or 100,000 cells/well in phenol red-free media. After a 1-h incubation at 37°C / 5% CO_2, media was discarded and replaced with BT. Fluorescence was measured at 37°C from the bottom of the wells with 485 ± 10 nm excitation and 528 ± 10 nm emission. Gain was adjusted to 5000. Background fluorescence was subtracted, and values for different groups were normalized to the values of non-transfected cells.

Results for (C): Whole-cell fluorescence of untransfected RBL-2H3 cells ("Plain RBL-2H3 control") (n=42 wells) and of ArcLight stably-transfected cells grown in hygromycin (+) (n=42 wells) or without hygromycin (-) (n=21 wells) was measured (C). Values are mean ± SEM of 7 independent experiments for hygromycin-exposed transfectants and control and 4 independent experiments for hygromycin-free transfectants. Statistical significance, represented by * $p<0.05$, was determined by a one-way ANOVA followed by a Tukey's *post-hoc* test. Stable transfectants' whole-cell fluorescence signal was not significantly different from RBL controls. This lack of ArcLight signal can be partially explained by the result that hygromycin exposure significantly reduces fluorescence in stable transfectants (C). Hygromycin is a protein synthesis inhibitor (Borovinskaya *et al.*, 2008): culturing transfectants in the presence of a protein synthesis inhibitor may decrease expression of the protein construct.

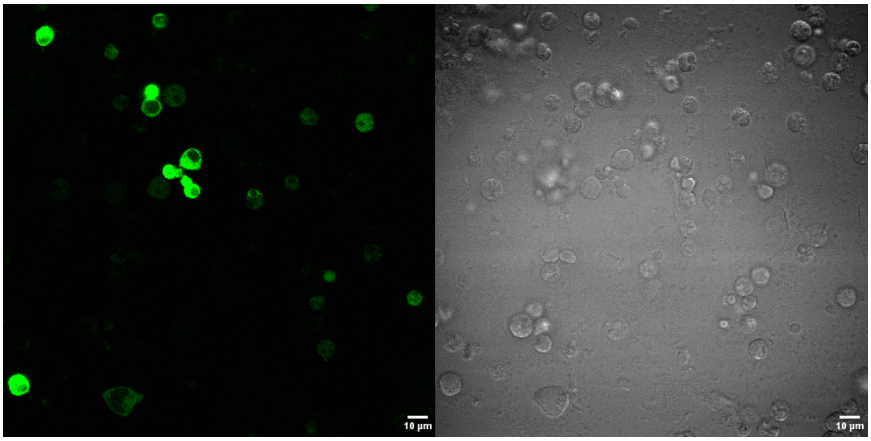

A) B)

Figure A.5. **Widefield images of GCaMP6-transfected Jurkat T cells.** Jurkat T cells were transfected with the GCaMP6 reporter construct and plated in fibronectin-coated ibidi plates in phenol red-free media, as described in Chapter 2. The next day, cell media was replaced with BT, and images were taken with a wide-field IX83 (Olympus) microscope as described in Chapter 2. Representative fluorescence (A) and DIC (B) images indicate high transfection efficiency of GCaMP6 in Jurkat T cells.

APPENDIX B

DIMETHYL SULFOXIDE VEHICLE DOES NOT INTERFERE WITH GRAMICIDIN'S INHIBITION OF PLASMA MEMBRANE POTENTIAL

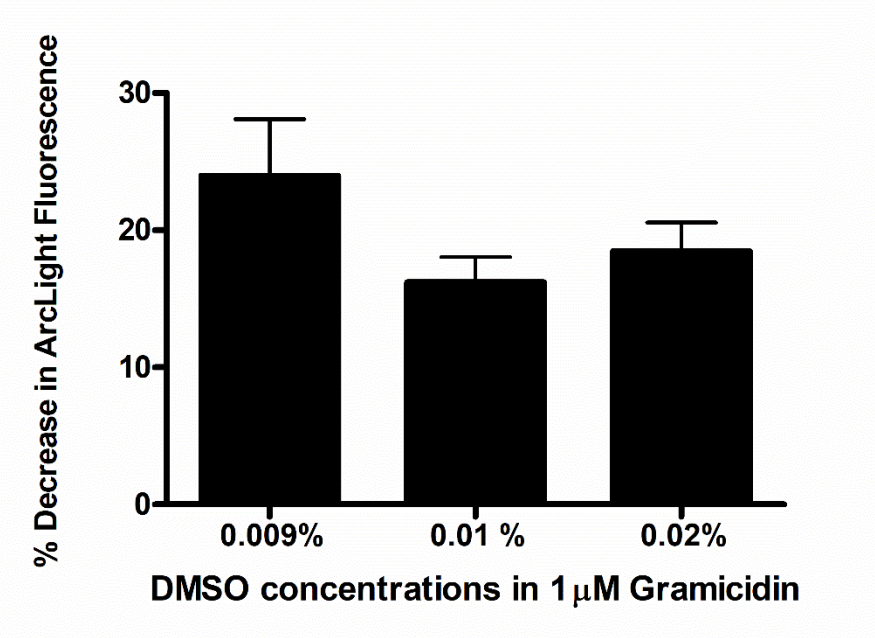

Figure B.1. Effects of DMSO vehicle on gramicidin's ability to decrease Arclight fluorescence in RBL mast cells. A range of DMSO concentrations was assessed to determine whether DMSO modulates gramicidin's ability to decrease Arclight fluorescence. RBL cells were transiently transfected with ArcLight, washed with BT, and exposed to 1 μM gramicidin dissolved in 0.009% (N=10), 0.01% (N=9), or 0.02% (N=5) DMSO (final concentration). Gramicidin-Arclight experiments were then performed as detailed in Chapter 2. For each individual cell, the percentage drop in ArcLight fluorescence mean intensity incurred by 7 min exposure to 1 μM gramicidin, in the presence of a certain DMSO concentration, was calculated, then averaged with values from other cells under the same conditions. Gramicidin's ability to inhibit Arclight fluorescence is unaffected by wide range of DMSO concentrations. Data presented are means ± SEM of at least 5 RBL cells per DMSO concentration. Analysis by one-way ANOVA followed by Tukey's post-hoc test found no statistical significance.

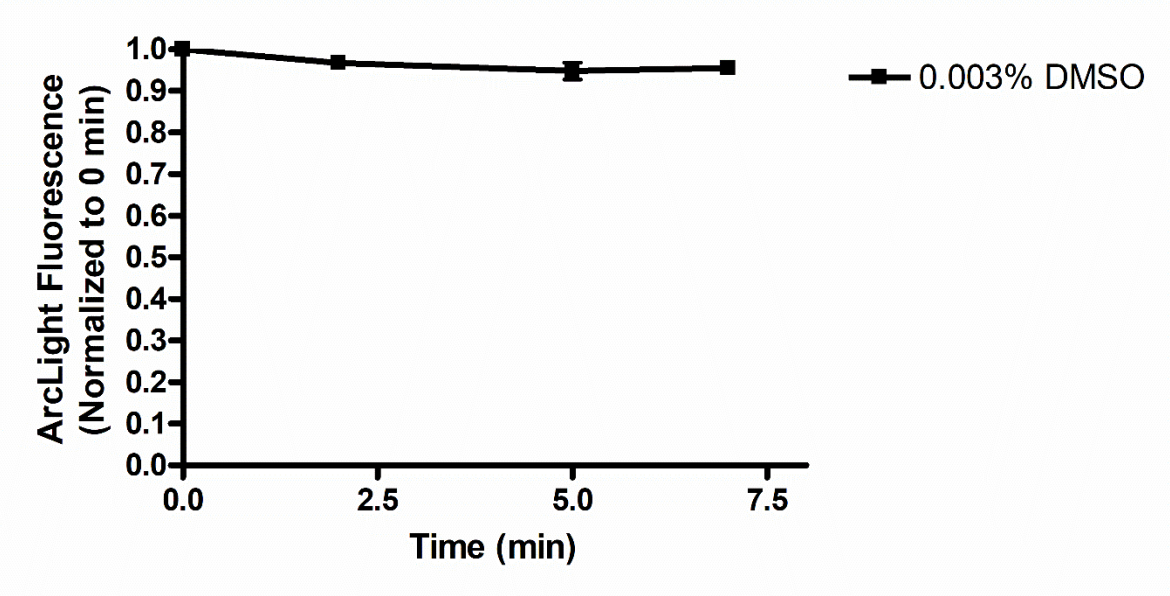

Figure B.2. Effects of DMSO vehicle on Arclight fluorescence. Since 1 μM gramicidin treatment in figure 3.3 contained DMSO vehicle (0.003%), it was important to determine whether 0.003% DMSO itself has any effects on ArcLight fluorescence under these experimental conditions. RBL cells were transiently transfected with ArcLight, washed with BT, and exposed to 0.003% DMSO (final concentration) in BT. Arclight experiments were then performed as detailed in Chapter 2. DMSO (at 0.003%) does not interfere with Arclight fluorescence. Values presented are means ± SEM from a single experimental day (N=6 cells). Analysis by one-way ANOVA followed by Tukey's post-hoc test found no statistical significance.

APPENDIX C

SUPPLEMENTARY INFORMATION TO CHAPTER 3

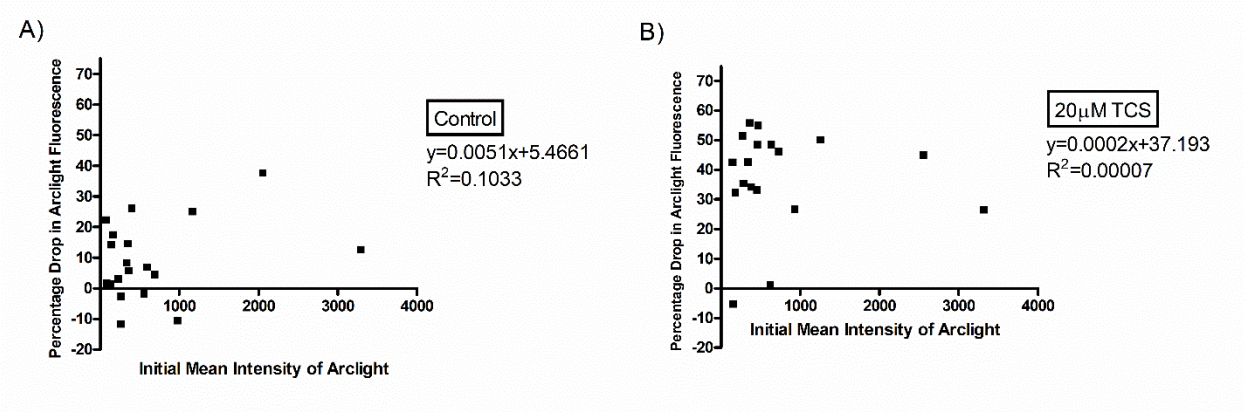

Figure C.1. Effect of cellular expression level of ArcLight-A242 on TCS inhibition of ArcLight-A242 fluorescence in human Jurkat T cells. To check whether plasmid expression level affects the change in GEVI fluorescence in response to triclosan in human Jurkat T cells, the initial, 0 min (pre-triclosan-exposure), background-subtracted mean fluorescence intensity of each individual cell from Figure 3.6A's data was analyzed. Data from Figure 3.6A, ArcLight-A242 transfected cells analyzed by confocal imaging and image analysis comparing control (0μM TCS) and 20μM TCS treatments, were plotted as individual cells' data. The percentage drop in ArcLight fluorescence by 15 minutes time of exposure (for control buffer-treated in A, TCS-treated in B), for each individual cell, is plotted as a function of that particular cell's initial mean intensity of ArcLight. There is no correlation between plasmid expression level and the magnitude of TCS inhibition of ArcLight fluorescence (Figure C.1B), as analyzed by linear regression. Thus, TCS effects on GEVI fluorescence are unaffected by the "brightness" (GEVI expression level) of the cell. Statistical results per plot are represented by equation of linear regression and corresponding R^2 values.

APPENDIX D

CALCIUM OSCILLATIONS IN JURKAT T CELLS

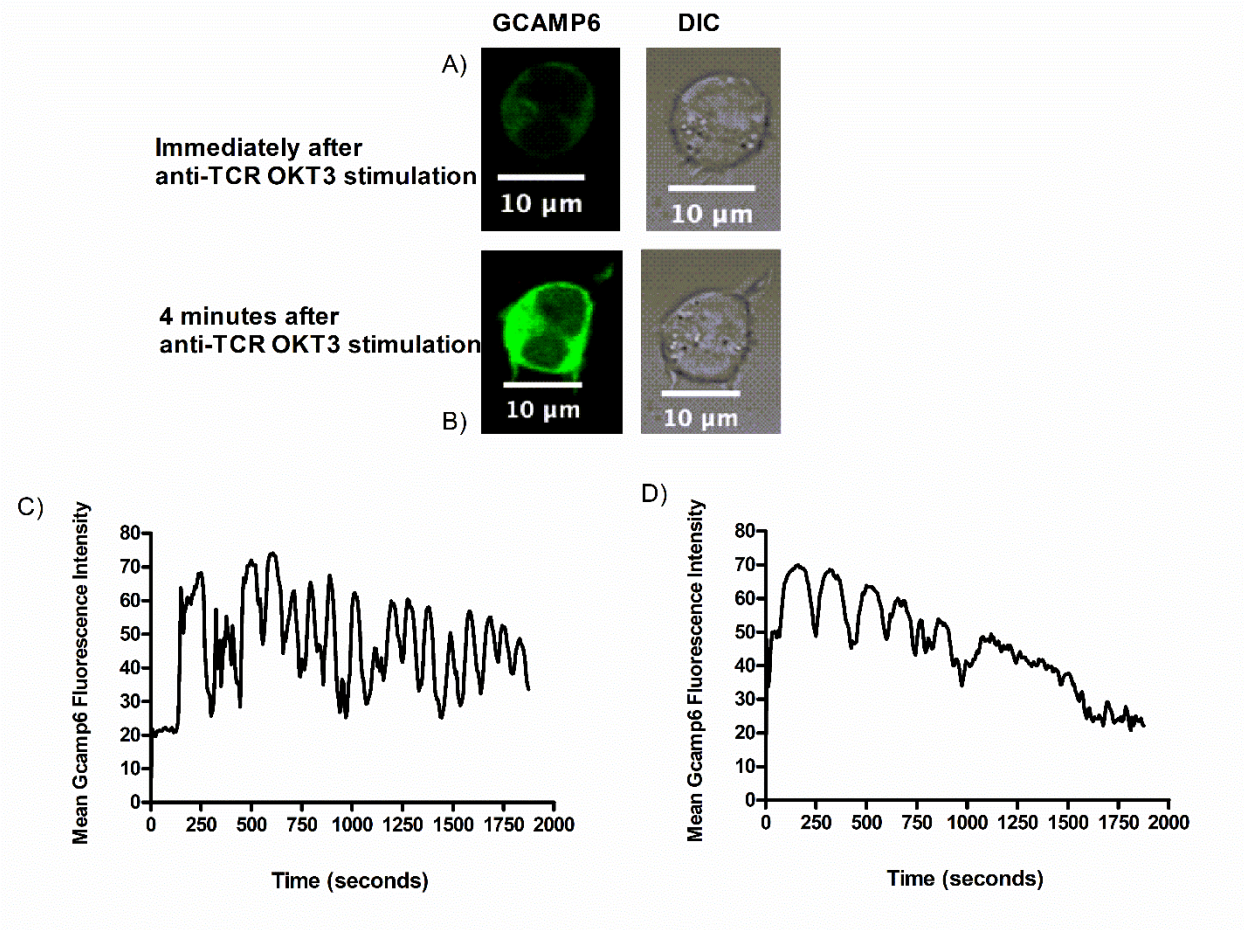

Figure D.1. Cytosolic Ca^{2+} levels as activated by anti-T Cell Receptor (TCR) antibody in individual Jurkat T Cells. Jurkat cells were transiently transfected with cytosolic GCaMP6 and exposed to 0.2 µg/ml anti-TCR OKT3 antibody. Representative live cell confocal microscopy images (fluorescence and DIC) from a single cell immediately **(A)** and 4 minutes **(B)** after antibody activation. Representative figures **(C and D)** (no error bars) show background-subtracted cytosolic mean fluorescence intensity of two individual cells for 30 minutes.

In order to investigate TCS inhibition of Ca^{2+} dynamics in T cells, we first visualized and quantified Ca^{2+} signaling in individual, antibody-activated cells. This technique could be used in future studies to investigate cellular Ca^{2+} oscillations.

Figure D.1. Visualizing and measuring Ca^{2+} oscillations in Jurkat T cells.

Methods for (A) and (B): First, 8-well ibidi plates were coated with 150 µL/well fibronectin (166 µg/ml) prepared in PBS and incubated overnight in tissue culture incubator. The next day, Jurkat T cells were transfected with pGP-CMV-GCaMP6f (a gift from Douglas Kim & GENIE Project; Addgene # 40755; http://n2t.net/addgene:40755; RRID: Addgene_40755) (Chen *et al.*, 2013) using Jurkat-specific Amaxa Nucleofector transfection kit T (Lonza). The electroporated cells were plated in phenol red-free Jurkat cell media at ~1 million cells/well in the fibronectin pre-coated 8-well. Cells were grown for 16-24 hours at 37^{o}C/ 5% CO_2. The next day, cell media was removed carefully with a transfer pipette to avoid cell detachment and replaced with 200 µL BT. Right before imaging, cells were exposed to 200 µL 2x anti-TCR OKT3 monoclonal antibody prepared in BT (final concentration of 0.2 µg/ml) ((Holowka *et al.*, 2018). Confocal live cell time lapse images (collected every 6.24 seconds) were taken for 30 minutes post addition of anti-TCR antibody in combination with BT. An Olympus FV-1000 confocal microscope, with an Olympus IX-81 inverted microscope and a 30 milliwatt multi-argon laser was used to collect images. GCAMP6 was imaged using a 60x oil immersion objective with NA 1.4 and 488 nm excitation, 505-605 nm band pass emission filter.

Results for (A) and (B): Fluorescence and DIC images (left and right) of a single Jurkat T cell obtained immediately (A) and 4 minutes after (B) addition of Anti-TCR OKT3 antibody show a sharp rise in cytosolic Ca^{2+} levels due to antibody activation.

To further quantify these Ca^{2+} levels, fluorescence images were processed using Fiji image J.

Methods for (C) and (D): In Fiji Image J (NIH), background fluorescence intensity was subtracted from each image stack using pseudo flatfield correction. Next, by applying threshold, binary masks of the whole cell was created. These binary masks were then further eroded to select only the cytosol of cells. Newly-formed cytosolic binary masks were applied to transfected cells to obtain area of the ROI, integrated density, and mean fluorescence intensity values.

Background-subtracted mean fluorescence intensity was plotted at every 6.24 seconds (Frame 1) up to 30 minutes (Frame 300).

Results for (C) and (D): Two representative figures depict quantified background subtracted mean fluorescence intensity of cytosolic GCaMP6 in two individual Jurkat T cells up to 30 minutes post anti-TCR OKT3 antibody addition. These data indicate that cytosolic Ca^{2+}oscillations in Jurkat T cells after antibody stimulation can be captured through confocal microscopy. Similar Ca^{2+} oscillations trend in RBL cells and T cells were reported in (Millard *et al.*, 1988; Lioudyno *et al.*, 2008) . This technique is not high-throughput but can be potentially used in future studies of toxicant effects on T cell Ca^{2+} mobilization.

APPENDIX E

OTHER CYTOSOLIC pH INDICATORS

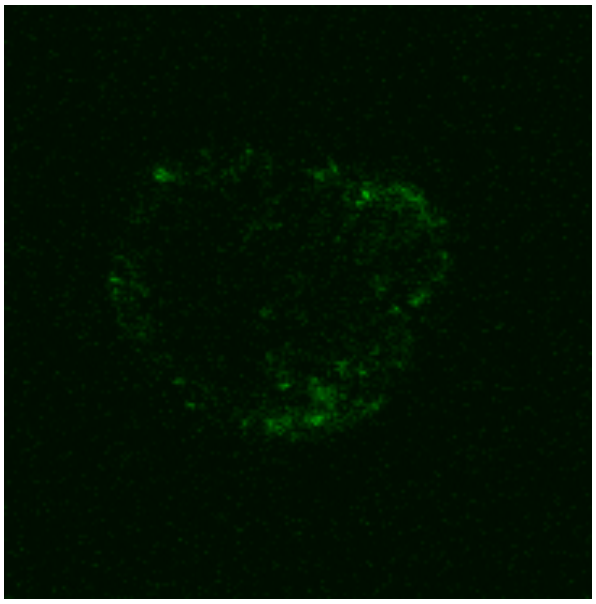

Figure E.1. Transfection of cytosolic pH marker pME-pHluorin2 into RBL mast cells. In order to investigate TCS effects on cytosolic pH, RBL cells were transiently transfected with pME-pHluorin2, which labels the cytosol and responds to pH changes with a change in its fluorescence (Mahon, 2011). The reporter construct pME pHluorin2 was a gift from David Raible (Addgene plasmid # 73794; http://n2t.net/addgene:73794; RRID:Addgene_73794) (Stawicki *et al.*, 2014). RBL cells were transfected similarly to how Lyn-tailed mCherry-SEpHlourin was transfected in Chapter 2. The next day, confocal images were taken in the presence of BT (confocal settings were similar to Arclight construct imaging as described in Chapter 2; timepoint images were not taken in this experiment). RBL cells transfected with the pME-pHluorin2 construct show a punctate cellular distribution, with highly uneven cytosolic labeling. Thus, this construct may not be useful to accurately measure cytosolic pH. Another cytosolic pH indicator known as pHRed (GW1-pHRed was a gift from Gary Yellen; Addgene plasmid # 31473 ; http://n2t.net/addgene:31473 ; RRID:Addgene_31473) (Tantama *et al.*, 2011), derived from red fluorescence protein, which also reports fluorescence change in response to changes in cytosolic pH, was available. However, pHRed does not detect any cytosolic pH change in response to 1 μM FCCP in Neuro2Acells (Tantama *et al.*, 2011). This result contradicts studies that show cytosolic acidification by FCCP (Buckler and Vaughan-Jones, 1998; Berezhnov *et al.*, 2016). Thus, we conclude that pHRed might not be a good pH indicator to measure TCS effects.

APPENDIX F

CYTOTOXIC EFFECTS OF CETYLPYRIDINIUM CHLORIDE IN NIH-3T3 CELLS

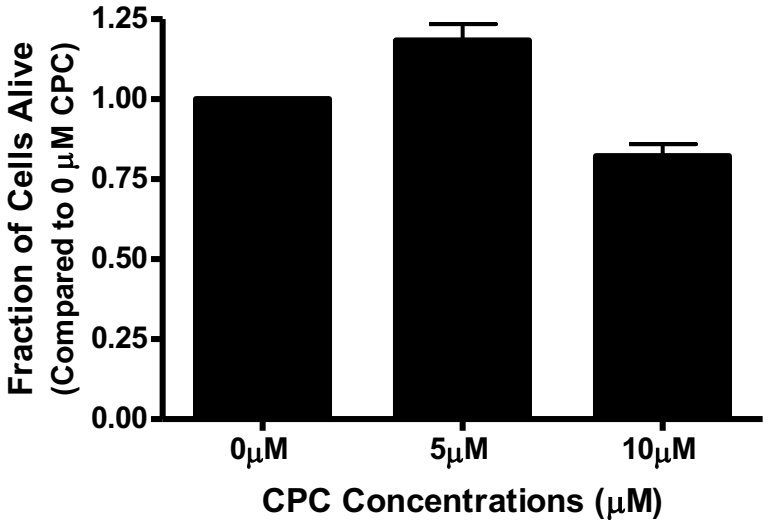

Figure F.1. Cytotoxic effects of cetylpyridinium chloride (CPC) on NIH-3T3 cells.

CPC is a widely used antimicrobial product which has been effectively banned recently from hand soaps and hand sanitizers by the FDA (Kux, 2016a; Kux, 2019), similarly to triclosan. CPC remains in numerous consumer products, at high concentrations. Because very little is known about CPC effects on eukaryotic cells, outside of its mitochondrial toxicity (Datta *et al.*, 2017), our lab has been focused on mapping the molecular mechanism by which it affects mammalian cells. CPC cytotoxicity was tested in NIH-3T3 cells to add context to microscopy data utilizing this cell line (to be published in a separate manuscript).

CPC (99% purity, VWR; CAS no. 123-03-5) was prepared in BT (Hutchinson *et al.*, 2011) by sonication (Branson 1200 ultrasonic cleaner; Branson Ultrasonics, Danbury, CT, USA) at 150 μM and 37 °C for 20 min, protected from light. Concentrations were determined using UV-Vis spectrophotometry (Weatherly *et al.*, 2013) and the Beer-Lambert equation ($A_{260} = \varepsilon_{260} \ell c$), using an ε_{260} of 4389 M^{-1} cm^{-1} (Bernauer, 2015).

NIH-3T3 cells were cultured as in (Weatherly *et al.*, 2016). Cells were plated at 200,000 cells per well into each of 3 wells of a 6 well plate (Greiner) and grown overnight at 37°C/5% CO_2. Next day, cells were exposed to micromolar doses of CPC (0 μM, 5 μM, and 10 μM) and incubated for 1 hour at 37°C/5% CO_2. Cell viability were assessed using a trypan blue exclusion assay (as in section 2.1.4). Values presented are means ± SEM of three independent experiments. Analysis by the nonparametric Kruskal-Wallis test followed by Dunn's post test found no statistical significance of either CPC dose compared to control. CPC (up to 10 μM, 1 hr) exposure does not cause cytotoxicity of NIH-3T3 cells.

BIOGRAPHY OF THE AUTHOR

Suraj Sangroula was born in a small village of Jhapa district in Nepal. In 2011, he moved to the United States with his family. He attended Concord High school for two years and graduated from there in 2013. After that, he attended the University of New Hampshire (UNH) at Durham, NH for a bachelor's degree in Biochemistry, Molecular and Cellular biology. During his time as an undergraduate, he received a scholarship to conduct an independent research project and presented his work at many national conferences. Suraj was also involved in many student organizations such as Best buddy UNH, Indian Subcontinental Student Association, Nepali Student Association. After finishing his bachelor's in 2017, he joined Dr. Julie Gosse 's lab at the University of Maine for his graduate degree. Suraj has one coauthored publication and one manuscript submitted to *Toxicology and Applied Pharmacology* for his first-author publication. He has presented his work at the Society of Toxicology (SOT) conference in Baltimore. During his first year of graduate school, he was also awarded scholarships to attend the quantitative fluorescence microscopy course at the Mount Desert Island Biological Laboratory. Suraj was a teaching assistant, teaching courses like Fundamentals of Chemistry and Biochemistry Laboratory. After receiving his degree, Suraj will move to Cincinnati, OH where his parents are living right now. Suraj is a candidate for the Master of Science degree in Biochemistry from the University of Maine in August 2020.